MARTIN MARIETTA ENERGY SYSTEMS LIBRARIES

3 4456 0280525 8

ORNL/TM-10666

ornl

OAK RIDGE
NATIONAL
LABORATORY

MARTIN MARIETTA

High Energy Resolution Measurement of the ^{238}U Neutron Capture Yield from 1 keV to 100 keV

Roger L. Macklin
R. B. Perez
G. de Saussure
R. W. Ingle

OAK RIDGE NATIONAL LABORATORY
CENTRAL RESEARCH LIBRARY
CIRCULATION SECTION
4500N ROOM 175
LIBRARY LOAN COPY
DO NOT TRANSFER TO ANOTHER PERSON
If you wish someone else to see this report, send in name with report and the library will arrange a loan.

OPERATED BY
MARTIN MARIETTA ENERGY SYSTEMS, INC.
FOR THE UNITED STATES
DEPARTMENT OF ENERGY

Printed in the United States of America. Available from
National Technical Information Service
U.S. Department of Commerce
5285 Port Royal Road, Springfield, Virginia 22161
NTIS price codes—Printed Copy: A04; Microfiche A01

This report was prepared as an account of work sponsored by an agency of the United States Government. Neither the United States Government nor any agency thereof, nor any of their employees, makes any warranty, express or implied, or assumes any legal liability or responsibility for the accuracy, completeness, or usefulness of any information, apparatus, product, or process disclosed, or represents that its use would not infringe privately owned rights. Reference herein to any specific commercial product, process, or service by trade name, trademark, manufacturer, or otherwise, does not necessarily constitute or imply its endorsement, recommendation, or favoring by the United States Government or any agency thereof. The views and opinions of authors expressed herein do not necessarily state or reflect those of the United States Government or any agency thereof.

ORNL/TM-10666

Engineering Physics and Mathematics Division

HIGH ENERGY RESOLUTION MEASUREMENT OF THE ^{238}U NEUTRON CAPTURE YIELD FROM 1 keV TO 100 keV

Roger L. Macklin,* R. B. Perez,**
G. de Saussure,** and R. W. Ingle***

*Nuclear Engineering Department, University of Tennessee
**Nuclear Engineering Department, University of Tennessee, and EPMD
***Instrumentation and Controls Division

DATE PUBLISHED — January 1988

Prepared for the
Office of Basic Energy Sciences
University Support Program

NOTICE: This document contains information of a preliminary nature. It is subject to revision or correction and therefore does not represent a final report.

Prepared by the
OAK RIDGE NATIONAL LABORATORY
Oak Ridge, Tennessee 37831
operated by
MARTIN MARIETTA ENERGY SYSTEMS, INC.
for the
U.S. DEPARTMENT OF ENERGY
under contract DE-AC05-84OR21400

MARTIN MARIETTA ENERGY SYSTEMS LIBRARIES

3 4456 0280525 8

CONTENTS

ACKNOWLEDGMENTS v
ABSTRACT vii
1. INTRODUCTION 1
2. DESCRIPTION OF THE EXPERIMENT 3
2.1 PRINCIPLE OF THE MEASUREMENT 3
2.2 EXPERIMENTAL ARRANGEMENT 3
2.3 THE DETECTOR 5
2.4 THE ELECTRONICS 9
2.5 THE DATA ACQUISITION SYSTEM 11
2.6 MULTIPARAMETER TOF-PULSE-HEIGHT SYSTEM 12
3. ANALYSIS OF THE DATA 17
3.1 DEAD-TIME CORRECTION 17
3.2 ENERGY CALIBRATION AND EXPERIMENTAL RESOLUTION . 18
3.3 BACKGROUND SUBTRACTION 21
3.3.1 Treatment of the Energy-Dependent Background 22
3.3.2 Treatment of the Constant Background Component 27
3.4 DETERMINATION OF THE NEUTRON BEAM SPECTRUM . . 28
3.5 NORMALIZATION OF THE CAPTURE YIELD DATA 30
3.6 UNCERTAINTIES IN THE MEASUREMENTS 34
4. RESULTS AND DISCUSSION 37
5. SUMMARY AND DISCUSSION 50
6. APPENDIX A 52
6.1 SAMPLE THICKNESS CORRECTIONS FOR WEAK CAPTURE RESONANCES IN ^{238}U IN THE NORMALIZATION REGION (600 EV - 1100 EV) 52
REFERENCES 54

ACKNOWLEDGMENTS

The authors are indebted to the operating staff of ORELA for the accelerator operation. The authors are grateful to J. A. Harvey and M. Moxon for their suggestions and advice on various aspects of the data analysis. Many thanks are due to R. L. Macklin for his advice, criticism, and his freely given wisdom on data analysis and interpretation. Two of us (RLM and RBP) are particularly indebted to Dr. S. L. Whetstone, DOE-Washington, for his advice and support through the University Support Program, U.S. Department of Energy, under grant DE-FG05-85ER90188.

ABSTRACT

The purpose of this work is the precise determination of the ^{238}U neutron capture yield (i.e., the probability of neutron absorption) as a function of neutron energy with the highest available neutron energy resolution. The motivation for this undertaking arises from the central role played by the ^{238}U neutron capture process in the calculation of the neutron balance of both thermal reactors and fast breeder reactors. The present measurement was performed using the Oak Ridge Electron Linear Accelerator (ORELA) facility.

The pulsed beam of neutrons from the ORELA facility is collimated on a sample of ^{238}U. The neutron capture rate in the sample is measured, as a function of neutron time-of-flight (TOF), by detecting the gamma rays from the $^{238}\mathrm{U}(n,\gamma)^{239}\mathrm{U}$ reaction with a large gamma-ray detector surrounding the ^{238}U sample. At each energy, the capture yield is proportional to the observed capture rate divided by the measured intensity of the neutron beam. The constant of proportionality (the normalization constant) is obtained as the ratio of theoretical to experimentally measured areas under small ^{238}U resonances where the resonance parameters have been determined from high resolution ^{238}U transmission measurements. The cross section for the reaction $^{238}\mathrm{U}(n,\gamma)^{239}\mathrm{U}$ can be derived from the measured capture yield if one applies appropriate corrections for multiple scattering and resonance self-shielding.

The present work will allow the extension of the resolved resonance region in ^{238}U from its current limit of 4 keV up to 20 keV. In addition, some 200 ^{238}U neutron resonances in the energy range from 250 eV to 10 keV have been observed which had not been detected in previous measurements. These results are relevant for both reactor design and for the understanding of the structure of the (^{238}U + n) compound nucleus.

1. INTRODUCTION

Though the ^{238}U capture cross section is known to ±5% between 30 and 500 keV,[1] the uncertainty is as large as ±10% between 1 and 30 keV. In particular,

1. The spread in the differential data is greater than expected from the assigned errors, especially below 30 keV.
2. The differential data do not meet the accuracy of ±3% or less required by the designers[2] of liquid-metal fast-breeder reactors (LMFBRs) and high-temperature gas-cooled reactors (HTGRs).
3. Integral measurements in fast reactors seem to imply values of effective ^{238}U capture cross sections which are ~10% lower than the values that are calculated from the best estimates based on differential data.

These inconsistencies in the ^{238}U capture cross section, which were discussed at the Antwerp Conference on Nuclear Data for Science and Technology in September 1982, led to the formation of the ^{238}U Task Force for the Nuclear Energy Agency Nuclear Data Committee (NEANDC).

The ^{238}U Task force[3] was set up to deal with two problems: (1) disagreement among the neutron widths of the resolved resonances above 1.4 keV (derived from transmission measurements at several laboratories, and (2) the ^{238}U capture cross section in the resolved and unresolved resonance regions. Among the most relevant conclusions arrived at by the NEANDC Task Force were that most of the capture cross-section measurements in the lower energy range (~1 to 30 keV) were old[4–8] and that they disagreed among themselves by more than expected from their respective error assignments.[9–11] To cope with these long-standing discrepancies, the ^{238}U Task Force[3] issued the following recommendations:

1. Reanalysis of the old ^{238}U capture data would be impossible, hence new measurements are required.
2. A high-resolution capture cross-section measurement (~150 m flight-path length) is urgently needed.
3. Previous inconsistencies in the normalization of the capture cross section in the 1- to 30-keV neutron-energy range must be resolved.

4. Extension of the evaluated resolved resonance energy range to higher energies. This would allow a consistent analysis of high-resolution transmission and capture data in the energy region between 1 and ~10 keV.

In response to these requests, a measurement of the ^{238}U capture yield was performed at the 150-meter flight-path station of the Oak Ridge Electron Linear Accelerator (ORELA) facility.[12] The present experiment has utilized ORELA as a powerful pulsed neutron source which, combined with the long (150-m) flight path, allows achievement of adequate energy resolution up to at least 20 keV. To obtain good statistical accuracy with low backgrounds, the large liquid scintillator tank (ORELAST) with an internal septum was used as a detector for capture gamma rays from the $^{238}\mathrm{U}(n,\gamma)^{239}\mathrm{U}$ reaction. The septum in the tank provides isolation of the signals from the left and right halves of the capture gamma-ray detector. Electronically requiring a time coincidence between the two halves drastically reduces the background from single ionizing events, yet it still leaves the response to capture gamma-ray cascades adequately high.[4]

The content of this work is organized as follows. Section 2 describes the principle of the measurement and gives detailed information on the experimental arrangement such as the detectors and electronic set-up. The methodology used for the analysis of the experimental data and the uncertainty analysis is described in Section 3. The capture yield results and comparisons with other measurements are given in Section 4.

2. DESCRIPTION OF THE EXPERIMENT

This section describes the experimental setup, methods, and instrumentation used for the determination of the ^{238}U capture yield.

2.1 PRINCIPLE OF THE MEASUREMENT

A pulsed beam of collimated neutrons impinges on a sample of ^{238}U. The neutron capture rate in the sample is measured, as a function of neutron time-of-flight (TOF), by detecting the gamma rays from the $^{238}\mathrm{U}(n,\gamma)^{239}\mathrm{U}$ reaction with a large gamma-ray detector surrounding the ^{238}U sample. At each energy, the capture yield is proportional to the observed capture rate divided by the measured intensity of the neutron beam. The constant of proportionality (the normalization constant) is obtained as the ratio of theoretical to experimentally measured areas under small ^{238}U resonances where the resonance parameters have been determined from high resolution ^{238}U transmission measurements.[13] The cross section for the reaction $^{238}\mathrm{U}(n,\gamma)^{239}\mathrm{U}$ can be derived from the calculated capture yield if one applies appropriate corrections for multiple scattering and resonance self-shielding.

2.2 EXPERIMENTAL ARRANGEMENT

The Oak Ridge Electron Linear Accelerator (ORELA)[12,14] was used to produce a pulsed source of neutrons. Pulses of approximately 140 MeV electrons of 12-A peak intensity impinge on a water-cooled tantalum target where they produce intense bremsstrahlung gamma rays which, in turn, generate neutrons by the (γ,n) reaction. Some of these neutrons are slowed down to the energies of interest by a water moderator surrounding the target assembly. This water is contained in a 2.4-mm-thick beryllium housing. The target-moderator assembly[15] is shown in Fig. 1.

The capture gamma-ray detector was positioned in the 150-m station of flight path 6 of ORELA. This flight path is normal to the surface of the moderator. The ^{238}U sample was placed at the center of the capture gamma-ray detector at a nominal distance of 151.96 m from the neutron source. The incident neutron detector was located between the ^{238}U sample and the neutron source at a nominal distance of 150.86 m from the latter.

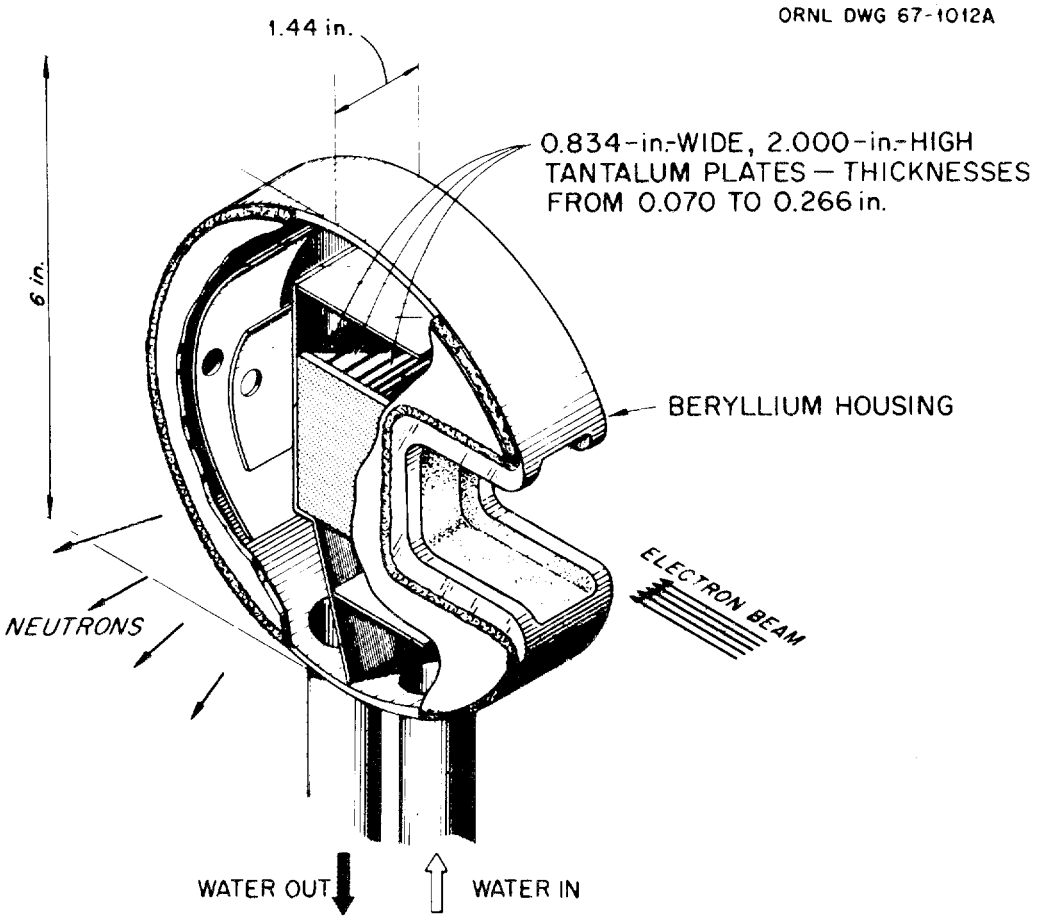

ORELA Be CLAD TANTALUM TARGET ASSEMBLY

Fig. 1. The High Power (50 kW) Water-Cooled Tantalum Neutron Target and Moderator Assembly for ORELA.

The neutron collimator system of flight path 6 has been described in detail by Silver et al.[16] and is shown in Fig. 2. The collimators are made of copper and lead to avoid the energy degradation caused by neutron scattering in lighter materials such as boron, lithium, or paraffin. The neutron beam is collimated to a 7.6-cm-diameter umbra at the sample position with an 8.2-cm-diameter penumbra. A shadow bar, rectangular in cross section and comprised of 61 cm of copper followed by 16 cm of lead, was positioned 2.5 m from the ORELA target to shield the ^{238}U sample from the bremsstrahlung radiation generated by the electrons impinging upon the tantalum target. This bar considerably reduces the "gamma flash" due to the gamma rays and unmoderated neutrons which would arrive at the detector a few microseconds after the electron burst strikes the target.

2.3 THE DETECTOR

The ORELA liquid scintillator tank (ORELAST)[16] is located on a flight path of 150 meters and serves as the detector for capture gamma rays in this measurement of the ^{238}U capture yield. A sketch of this detector is shown in Fig. 3. The tank contains approximately 3000 liters of solution, consisting of three parts commercial liquid scintillator[17] (NE-224) to one part trimethylborate. The function of the trimethylborate additive is to reduce background counts arising from the 2.22-MeV capture gamma ray in hydrogen. Thus, scattered neutrons which are thermalized in the solution can be captured by boron rather than hydrogen. Approximately 96% of the neutrons captured in boron result in a 0.478-MeV gamma ray.

The surface of the ORELAST tank is studded with 32 RCA Model 4522 photomultiplier tubes which are positioned to cover equal surface areas of the liquid scintillator. The gain for each photomultiplier tube is individually adjusted to provide optimum overall pulse-height resolution of the detector. The ORELA neutron beam passes through an aluminum tube which traverses the ORELAST tank and in which the ^{238}U sample is centered. A liner composed of a lithium hydride annular cylinder (152.6-cm length and 2.5-cm thickness) is placed inside the through-tube, serving to further reduce the background caused by neutrons scattering off the ^{238}U sample and decreasing the probability of fast neutrons scattered by the scintillator which might return to the ^{238}U sample.

The ORELAST tank is optically divided into two equal halves by 0.05-mm-thick aluminized-mylar sheets in the vertical plane which contains the neutron-beam

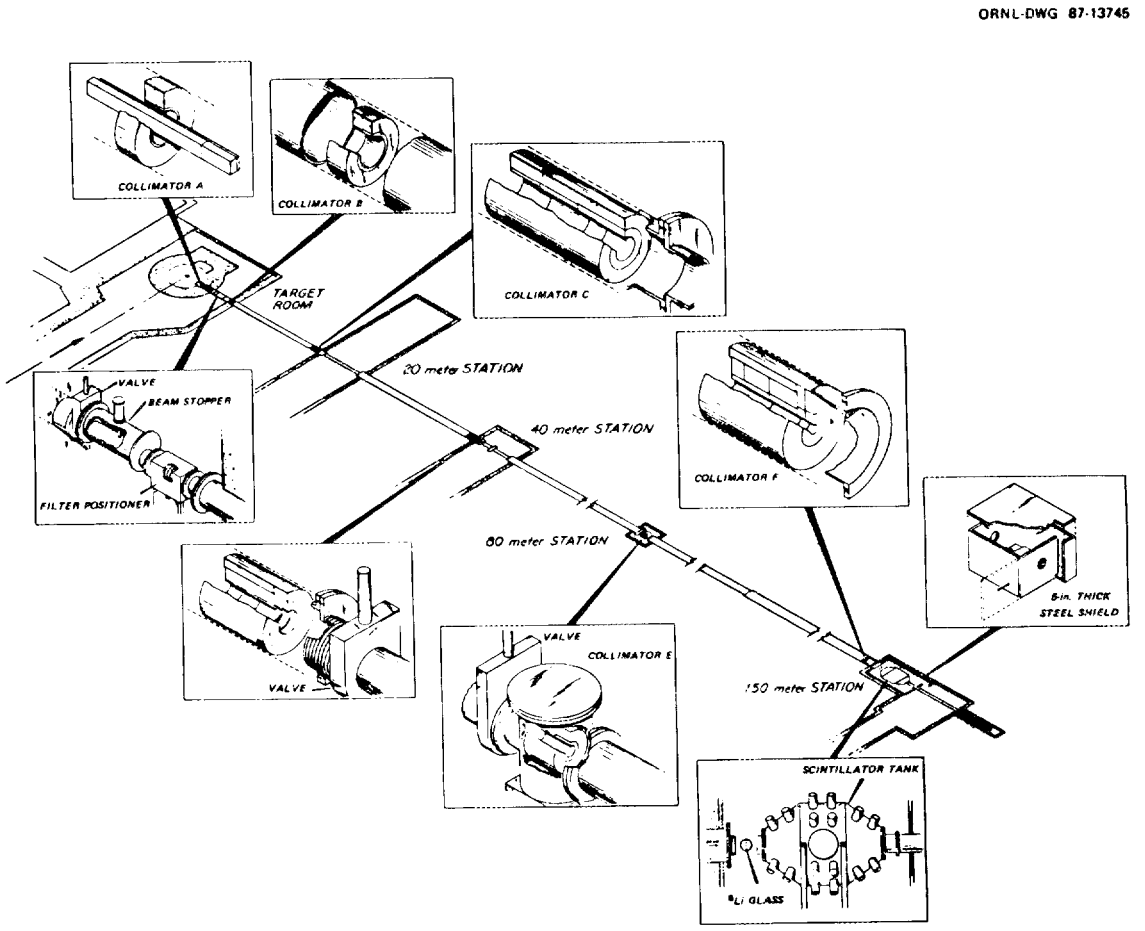

Fig. 2. The Collimation System for the 150-meter Station of Flight Path 6 at the ORELA Facility, Showing in Particular the Beam Stopper, the Filter Positioner, and the Copper and Lead Collimators.

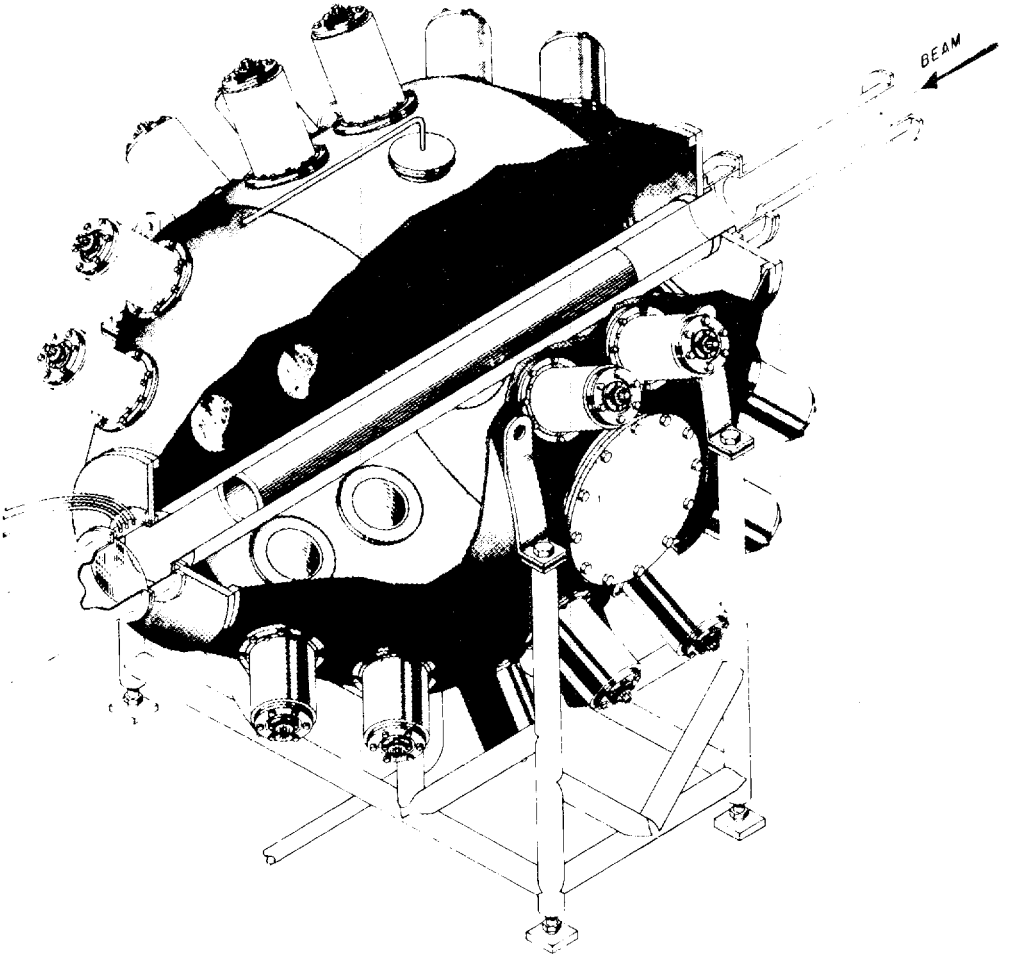

Fig. 3. Sketch of the ORELA Liquid Scintillator Tank (ORELAST). This tank is viewed by thirty-two 12.7-cm-diameter RCA Model 4522 photomultiplier tubes. It was separated into two equal sides with an aluminized mylar septum in the vertical plane containing the beam axis. This septum is not shown in the figure.

axis. Requiring coincidence between the signals from the two halves of the tank provides an approximately eight times higher signal-to-background ratio than could be obtained using "singles" mode. This takes advantage of the high multiplicity of gamma rays from neutron capture in the ^{238}U sample at the center of the tank, whereas the background is in large measure composed of single gamma rays which have a lower probability of being seen in both halves of the tank.

The ^{238}U circular samples used were one of 0.635-mm nominal thickness (65.47 grams in weight and 8.26-cm mean diameter), and a second of 2.54-mm nominal thickness (473.70 grams in weight and 11.11-cm mean diameter) (see Tables I and II). A particular sample is placed in a light aluminum holder and positioned at the center of the ORELAST tank inside the lithium-hydride liner. Both ends of the tank are sealed with mylar windows, and argon gas is passed continuously through the through-tube (because argon scatters fewer neutrons than air).

Table I. Isotopic Composition of the ^{238}U Metallic Samples

^{233}U	<1 ppm
^{234}U	<1 ppm
^{235}U	<5 ppm
^{236}U	<1 ppm
^{238}U	99.99%

Analysis provided by H. Gwinn, ORNL Isotopes Division.

Table II. Dimensions and weights of the ^{238}U metallic samples

Nominal thickness	25 mil		100 mil	
Mean diameter (cm)	8.26	± .043	11.11	± .058
Area (cm^2)	53.6	± .7	96.9	± 1.0
Weight (g)	65.470	± .012	473.90	± .09
Areal Density				
(g/cm^2)	1.222	± .016	4.887	± .064
(atoms/barn)	.00309	± .000046	.01236	± .00016

The neutron flux is measured by a ^{6}Li glass scintillator[18] positioned just "upstream" of the ORELAST tank. This detector is a disk of 83 mm diameter and 1 mm thickness (Nuclear Enterprises Co. type NE-912) mounted in a light-tight housing which is viewed by two RCA Model 4522 photomultiplier tubes.

2.4 THE ELECTRONICS

A simplified block diagram of the electronics system is shown in Fig. 4. The fast signals from the anodes of 16 photomultiplier tubes are summed and then amplified for each side of the tank. The outputs from these modules are coupled to separate constant fraction discriminators which are then fed to a coincidence circuit which produces an output only when both sides of the tank detect the capture gamma rays.

The linear signal from the tank comes from the dynodes of the photomultiplier tubes, all 32 of which are summed together. This signal is processed by a Tennelec model TC-200 linear amplifier. The output from this amplifier is fed to the data-acquisition system in the data-processing lab and to a cross-over discriminator. This discriminator determines the gamma-ray pulse-height energy range over which the measurement is conducted (in this case, from 2.4 MeV to 10.4 MeV).

Signals from the "fast" coincidence circuit and the "slow" cross-over discriminator are coupled to a coincidence circuit. The "fast" signal determines the timing resolution, and the "slow" signal determines the gamma-ray energy range. The output from this coincidence circuit is presented to the data-acquisition system as a timing pulse.

The timing signal from the ^{6}Li glass neutron-flux detector is derived in a similar manner. Two RCA model 4522 photomultiplier tubes, one at each side of the lithium glass scintillator and well clear of the neutron beam, view the light output induced by the alpha particle and triton of the $^6\mathrm{Li}(n,\alpha)\mathrm{T}$ reaction. Anode signals are processed by fast sum and discriminator circuits. The discriminator bias window is set just below and just above the peak from the $^6\mathrm{Li}(n,\alpha)\mathrm{T}$ reaction. (Both the alpha particle and the tritium nucleus produce light output since both are charged particles.)

A small ^{252}Cf fission chamber with a fission count rate of 65 per second is also placed in the lithium hydride through-tube liner slightly "downstream" of the ^{238}U sample but below the neutron beam. The fission fragment signal from the

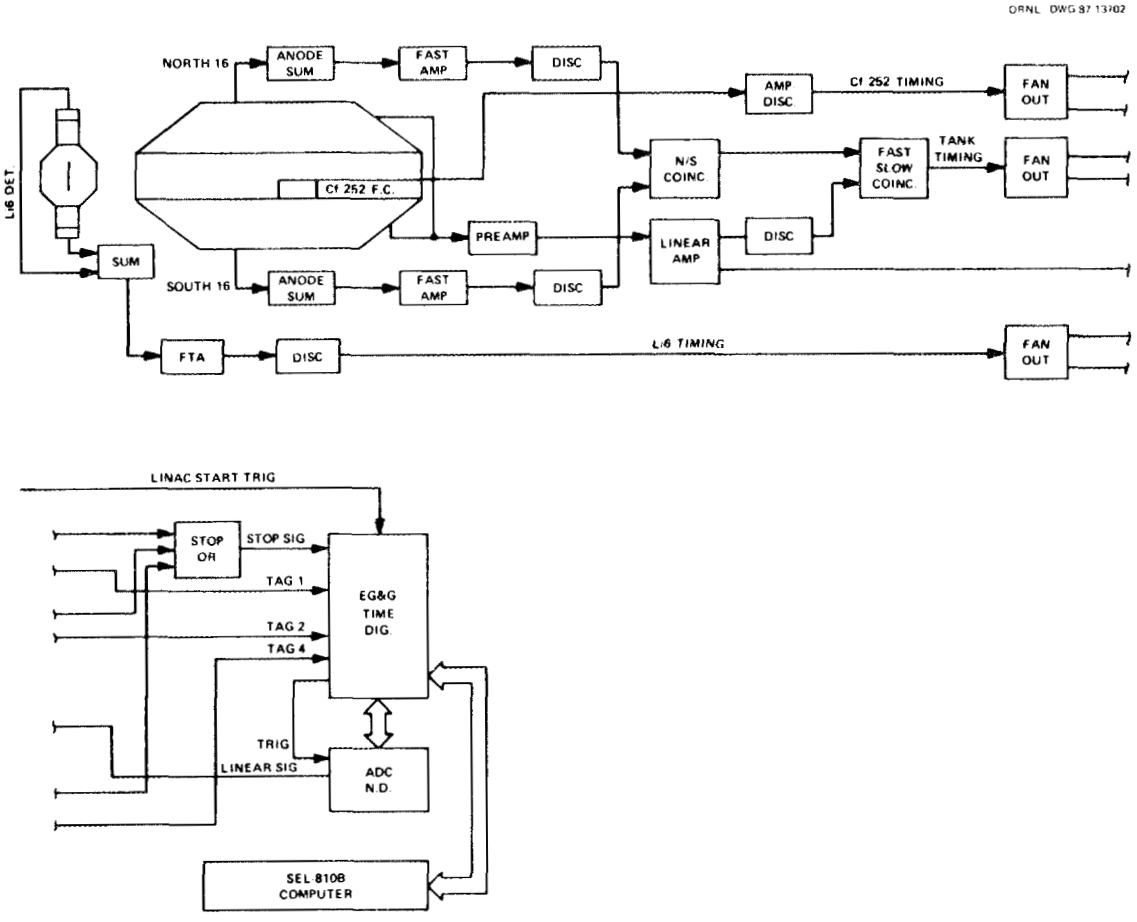

Fig. 4. Simplified Block Diagram of the Electronic Circuitry Used in the Measurements of the ^{238}U Capture Yield. The time-of-flight spectra were accumulated on a fast random access disk linked to the SEL Model 810-B computer and later unloaded on magnetic tape and analyzed on a DEC Model VAX 11/785 computer by batch process.

amplifier-discriminator circuit is used to monitor continuously the tank timing and gain. The full-width-at-half-maximum (FWHM) of the coincidence time spectrum between the ^{252}Cf and the scintillator tank is approximately 6 nanoseconds.

The timing and pulse-height information are processed simultaneously in the data-acquisition lab. The neutron time-of-flight is measured using an EG&G model TDC-100 multistop time digitizer. The start trigger for this device is derived from the linear accelerator (LINAC) gamma flash. Pulses from the scintillator tank, the neutron flux monitor, and the ^{252}Cf circuits are coupled to the TDC stop input.

Scintillator tank pulse-height information is derived from a Nuclear Data model 560 analog-digital converter (ADC). The binary information from the ADC and TDC are combined in the time digitizer and fed to a Systems Engineering Laboratories (SEL) model 810-B digital computer which stores the information (on disk).

The separate detector signals are presented to "tag" inputs in the TDC, allowing the computer to identify each signal.

2.5 THE DATA ACQUISITION SYSTEM

Binary information representing neutron time-of-flight, gamma-ray pulse height, and identification tags are combined to form a 30-bit word for each event which is read by the data-acquisition computer.

The ORELA data-acquisition computer system[19] consists of three SEL model 810-B digital computers used for on-line data acquisition, a peripheral equipment controller (also a SEL 810-B), and a DEC model VAX 11/785 digital computer used for data analysis. Each data-acquisition computer can simultaneously record data from four experimental systems. Data to the computers are handled by a priority multiplexing scheme with continuous input, and storage is accomplished using a fixed-head disk.

The data space available for the three SEL 810-B computers is 350K, 750K, and 1000K sixteen-bit words.

Programs for the data-acquisition computer are stored in core memory when active. The data-acquisition programs and system-monitor program are organized into the ORELA Data-Acquisition Monitor System.[20] The experimenter's data-acquisition program is commonly called a "crunch routine." Program constants that

determine time-channel width, pulse-height conversion gain, and multiparameter storage are entered to the program by a card reader or teletype.

2.6 MULTIPARAMETER TOF-PULSE-HEIGHT SYSTEM

For each sample and filter configuration, five TOF spectra were simultaneously recorded into five pulse-height bins. A time-of-flight, pulse-height multiparameter system was designed to monitor the TOF spectra signal-to-background ratios and to observe whether or not appreciable changes would occur in the TOF spectra due to electronic bias shifts and the energy dependence of the average properties of the gamma-ray cascade following neutron capture. Table III shows the pulse-height ranges (in MeV) used for this purpose, and Table IV gives the time-of-flight program which applies to each pulse-height bin, for an accelerator repetition rate of 800 pulses per second. The pulse-height spectrum was calibrated by measuring the gamma-ray pulse-height spectrum of a standardized ^{60}Co source.

Table III. Bias Levels for the TOF-Pulse-Height Multiparameter System

TOF Section	Pulse-height Range (MeV)
1	0.00 – 1.86
2	1.86 – 2.79
3	2.79 – 4.65
4	4.65 – 6.51
5	6.51 – 8.33

The pulse-height bin selection was performed by inspection of the pulse-height spectrum of the 518-eV resonance. Figure 5 shows the pulse-height spectrum measured at the neutron time-of-flight corresponding to the 518.3-eV ^{238}U resonance. The large spike seen in the figure is due to various background contributions (such as from the electronics, from radioactivity in the sample, etc.). This background contribution is seen in Fig. 6 which shows a pulse-height spectrum around 500 eV where there are no large resonances in the (^{238}U + n) compound nucleus. Examination of the background subtracted pulse-height spectrum in Fig. 7 shows that pulse-height bins 3 and 4 (see Table III) exhibit the best signal-to-background ratio. The TOF spectra for these two sections were separately analyzed, following the

procedure described in Section 3 of this work, in an effort to detect any systematic effects due to tank coincidence bias changes and the energy dependence of the gamma-ray cascades. None of these effects could be detected as they are probably overshadowed by the uncertainties in the background subtraction which are strongly dependent on the signal-to-background ratio which are, in turn, different for each pulse-height bin.

Table IV. Time-of-Flight Program for Measurement of ^{238}U Capture Yield (for Accelerator Repetition Rate of 800 Pulses per Second)

Number of Channels	Channel Width (nsec)	Time-of-Flight (μsec)	Energy (keV)
1000	32	0 – 32	2500 – 136.409
25000	4	32 – 132	136.409 – 7.168
10000	8	132 – 212	7.168 – 2.743
10000	16	212 – 372	2.743 – 0.883
10000	32	372 – 692	0.883 – 0.254

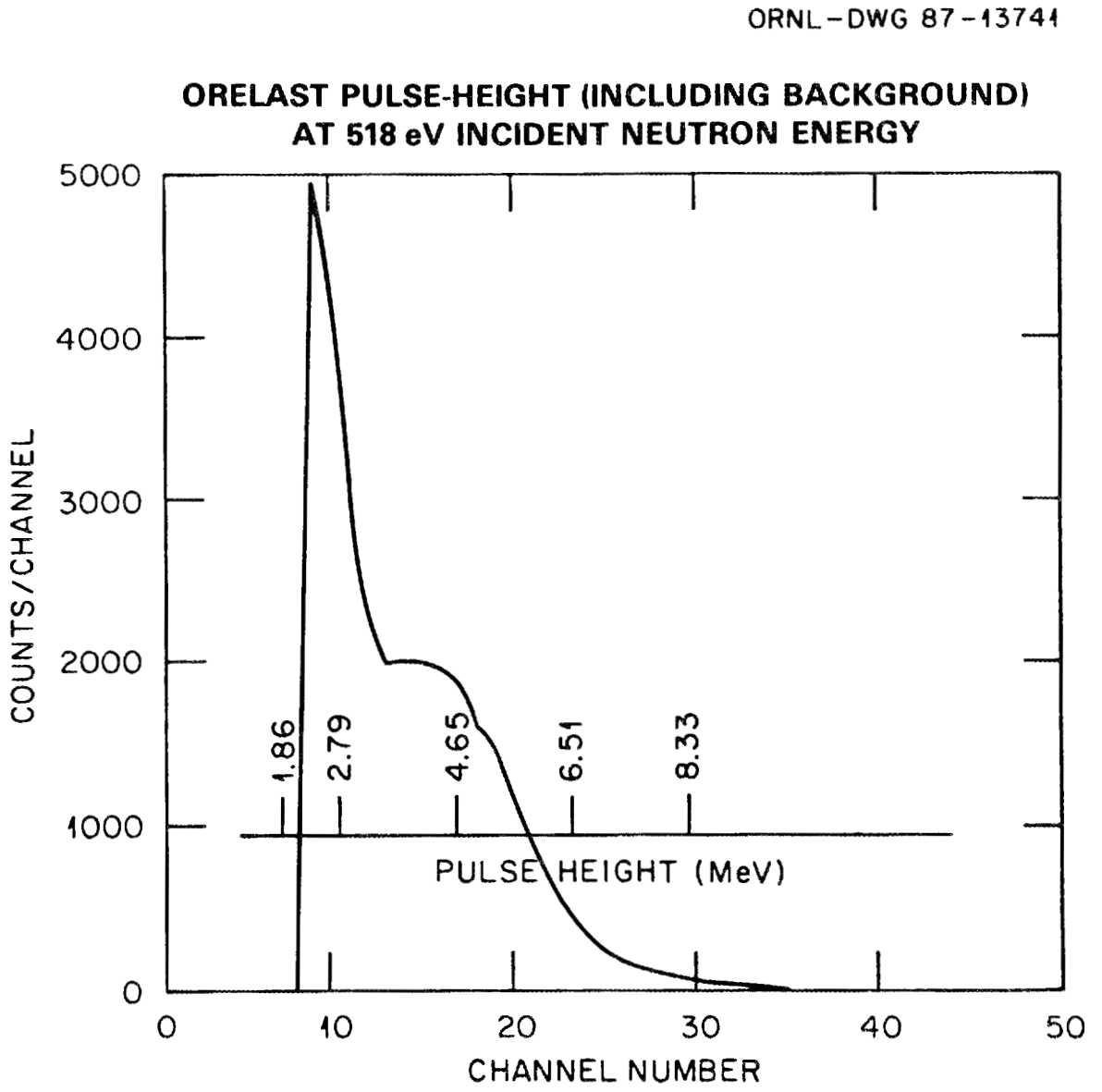

Fig. 5. ORELAST Pulse-Height Spectrum (Including Background) at TOF Corresponding to 518 eV, Showing Counts Versus Channel Number. The large spike is due to background contributions. The second horizontal scale shows the pulse-height ("bias") group boundaries.

ORNL-DWG 87-13742

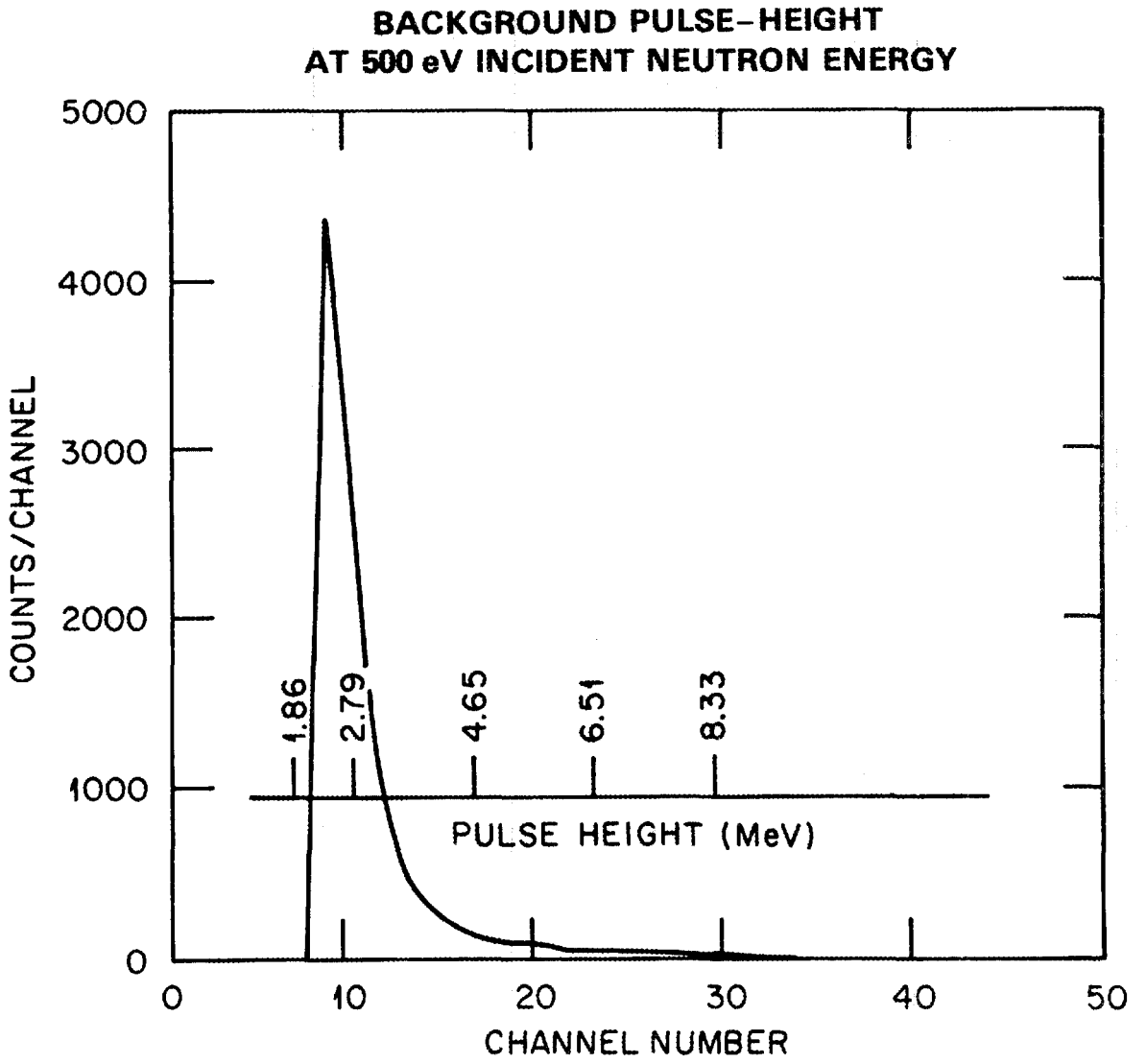

Fig. 6. ORELAST Pulse-Height Spectrum at TOF Corresponding to 500 eV, Showing Counts Versus Channel Number for the Background Contribution. The second horizontal scale shows the pulse-height ("bias") group boundaries.

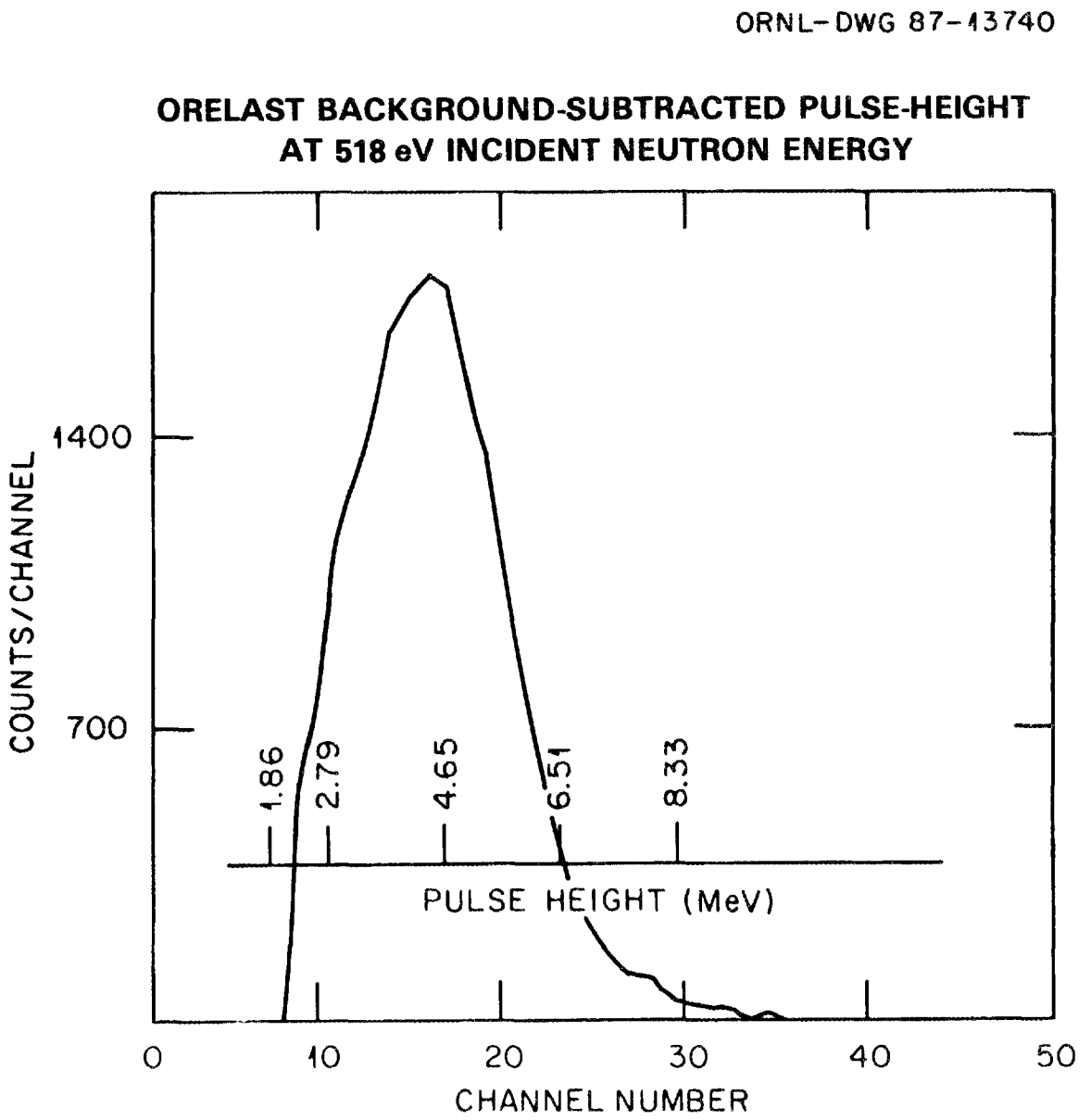

Fig. 7. ORELAST Pulse-Height Spectrum at TOF Corresponding to 518 eV, Where the Background Contribution Has Been Subtracted, Showing Counts Versus Channel Number. The second horizontal scale shows the pulse-height ("bias") group boundaries.

3. ANALYSIS OF THE DATA

The purpose of the analysis of the data is to obtain the capture yield, $Y_c(E)$ (i.e., the probability of neutron absorption), as a function of neutron energy for each of the ^{238}U samples used in this measurement. The capture yield is defined as a function of the neutron energy, E, by the relation

$$E^{1/2}Y_c(E) = a_n \left[\frac{C(E)}{S(E)}\right] R(E)(\mathrm{b} \cdot \mathrm{eV}^{1/2}) \qquad (3-1)$$

where

a_n = normalization constant.

$C(E)$ = background subtracted count rate from the ORELAST detector,

$S(E)$ = background corrected count rate from the lithium glass neutron flux monitor,

$R(E)$ = a factor which accounts for the deviation of the ^{6}Li(n,α) T cross section from $<< 1/v >>$ behavior,

Five measurements of the gamma-ray TOF spectrum were performed for each of the two ^{238}U samples. Measurements were done with and without aluminum filters in the neutron beam, at LINAC repetition rates of 800 and 400 pulses per second, to determine the energy-dependent background which arises from neutron-pulse overlap and room return. The fifth measurement was performed using a polyethylene filter in the beam to determine the energy independent ("constant") component of the background. A ^{10}B filter was used in all runs to reduce low-energy ($<$ 250 eV) neutrons from the "tail" of the previous pulse (pulse "overlap"). The successive steps in the data analysis to obtain the capture yield are discussed in detail below.

3.1 DEAD-TIME CORRECTION

All time-of-flight spectra were taken simultaneously for each sample using the same digital time-interval counter. Thus, the dead-time correction is the same for all TOF spectra for any given time-of-flight channel. However, this dead-time correction does not cancel in the ratio of the counts from the gamma-ray detector to those from the neutron-flux monitor (see Eq. 3-1) because the energy corresponding

to a given time-of-flight channel is not the same for the two detectors. A fixed dead-time of 32.768 microseconds (larger than the dead-time of any of the electronic components) was artifically imposed on the equipment. This arrangement allowed a straightforward calculation of the dead-time correction which was typically of the order of 1 to 2% and never exceeded 12%.

3.2 ENERGY CALIBRATION AND EXPERIMENTAL RESOLUTION

The conversion of measured time-of-flight, τ, to neutron energy is performed by the relation (neglecting relativistic effects)

$$E = \mu^2 \frac{L^2}{(\tau + \tau_0)^2} \text{ (eV)} \qquad (3-2)$$

where

μ = 72.3 $(\text{eV})^{1/2}(\mu\text{sec})/\text{m}$,
L = neutron flight path (m), and
τ_0 = initial delay of the time-of-flight "clock" due to delays in the electronics chain (μsec).

Rather than measuring L and τ_0, these two parameters were obtained by solving Eq. 3-2 for pairs of resonances of known energies in the uranium and aluminum nuclei. The resulting energy scales were then realigned with the precise energy calibration of Olsen et al.[13] Table V gives the values for L and τ_0, for each sample thickness, derived from this realignment.

Table V. Flight Path Distance and Initial Clock Delay for the ^{238}U Capture Yield Data as Derived from Alignment with Energy Scale of Olsen et al. (Reference 13)

Sample (atoms/barn)	Flight Path Distance, L (meters)	Initial Clock Delay, τ_0 (microseconds)
0.01236	151.939	−2.256
0.00309	151.947	−2.255

The experimental resolution broadening is well described[21] by a Gaussian convolution of width given by the expression

$$\Delta^2 = \Delta_D^2 + \Delta_M^2 + \Delta_t^2 \ , \qquad (3-3)$$

where Δ_D is the Doppler broadening width, Δ_M represents the broadening effect of the moderator, and Δ_t is the width associated with the timing resolution. These quantities are given by the relations[22–25]

$$\Delta_D^2 = \frac{4kTE}{A} \ , \qquad (3-4)$$

$$\Delta_M^2 = \frac{2}{3}\left[\frac{(s^2+\ell^2)}{L^2}\right] E^2 \ , \qquad (3-5)$$

and

$$\Delta_t^2 = \frac{2}{3}\left[\frac{(\tau_b^2+\tau_c^2)}{\mu^2 L^2}\right] E^3 \ , \qquad (3-6)$$

where

k = Boltzmann constant = 8.61781×10^{-5} (eV)(°K)$^{-1}$,
T = effective sample temperature = 300°K,
A = target mass number = 238,
s = "equivalent" moderator thickness (FWHM) = 2.16 cm,
ℓ = "equivalent"length corresponding to the neutron slowing-down time in the moderator (cm) = 2.63 cm,
τ_b = pulse width of the neutron burst (μsec) (typically of the order of 14 nsec), and
τ_c = channel width (μsec) (variable, from a minimum of 4 nanoseconds to a maximum of 32 nanoseconds.)

With the above parameters one obtains

$$\Delta_D = 2.08 \times 10^{-2} E^{1/2} \text{ (eV)} \ , \qquad (3-7)$$

$$\Delta_M = 1.83 \times 10^{-4} E \text{ (eV)} \ , \qquad (3-8)$$

and

$$\Delta_t = 7.42 \times 10^{-8} \left(196 + \tau_c^2\right)^{1/2} E^{3/2} \text{ (eV)} \ , \qquad (3-9)$$

with τ_c being the channel width in nanoseconds.

Table VI shows a comparison between the resolution widths of the nominal 40-meter flight-path measurement of de Saussure et al.[4] and the present measurement at the nominal 150-meter flight path. Note that below 10 keV, the Doppler broadening is the largest contribution, whereas above 10 keV the timing and moderator resolution effects are the dominant contributions to the overall resolution width in the case of the present measurement. However, for the 40-m flight-path measurement, the resolution width due to the moderator is the dominant contribution between 1 keV and 10 keV. Note that at neutron energies around 10 keV, the overall resolution width for an experiment with $L = 40$ m is three times the corresponding resolution width achievable at $L = 150$ m, and about half the average level spacing for s-wave resonances in the (^{238}U + n) compound nucleus.

Table VI. Comparison of Resolution Widths (eV) for two ORELA ^{238}U Neutron Capture Yield Measurements

Partial resolution widths (eV) at neutron energies of	1 keV	10 keV	100 keV
Doppler width (eV)	.66	2.1	6.6
Moderator width (eV)			
(a) 40 m	.70	7.0	70.0
(b) 150 m	.18	1.8	18.0
Timing width (eV)			
(a) 40 m	.15	4.2	133.5
(b) 150 m	.05	1.1	34.2
Overall resolution width (eV)			
(a) 40 m	.97	8.4	150.9
(b) 150 m	.69	2.9	39.2

(a) Measurement of de Saussure et al.[4]: $L = 39.7$ m; $\tau_c = 10$ nsec at 1 keV; $\tau_c = 5$ nsec above 1 keV.

(b) Present measurement: $L = 151.9$ m; $\tau_c = 16$ nsec at 1 keV: $\tau_c = 4$ nsec above 1 keV.

3.3 BACKGROUND SUBTRACTION

The time-of-flight (TOF) spectra obtained from the capture gamma-ray detector are contaminated by two background components—an energy-dependent component and a "constant" background contribution. The energy-dependent background arises from several sources:

1. Beam neutrons generated in previous neutron bursts (pulse overlap),
2. Room return neutrons which reach the ^{238}U sample, after a time longer than the inverse accelerator repetition rate,
3. Beam neutrons producing prompt gamma rays upon capture in materials around the detector.

The first two energy-dependent background sources have the common feature of arising from neutrons generated more than one pulse before detection. Their TOF spectrum, which is proportional to the energy-dependent background, can be obtained by running the pulsed neutron source at half the repetition rate, f_H, of the foreground run. Neutrons taking longer than $2/f_H$, which would also contribute to the background, fall in an energy range such that they are absorbed by the ^{10}B filter (199 g in weight and with areal density of 0.05577 atoms/barn). Hence, for each experimental configuration, two runs are performed: a "high frequency" run at a repetition rate of 800 pulses per second and a"low frequency" run at 400 pulses per second.[26] The third energy-dependent background contribution cannot be measured directly, but it can be minimized by the use of good neutron beam collimation.

The constant background component is produced by two sources: (1) cosmic rays, and (2) long-lived radioactivities in the detector, surrounding materials, and the ^{238}U samples.

The constant background component consisting of muons (generated in the atmosphere by cosmic rays) is considerably reduced through the orientation of the internal aluminized-mylar septum in the ORELAST detector. These muons have predominantly vertical tracks so that the vertical septum is clearly superior to a horizontal septum for rejecting this background component.

To determine the constant background contribution, a measurement was performed for each experimental configuration with a polyethylene plug (four contiguous 2.54-mm-thick pieces) inserted in the neutron beam. Below 100 keV, the polyethylene effectively removes the beam neutrons but is relatively transparent

to the gamma-ray background, which includes gamma rays produced by the accelerator ("gamma flash"), and gamma rays created in the water-cooled neutron moderator by the nuclear reaction $H + n \rightarrow D + \gamma$.

3.3.1 Treatment of the Energy-Dependent Background

Figure 8 shows TOF spectra for a high-frequency run (upper curve) and a low-frequency run (lower curve). Note that because of the different time-of-flight intervals spanned in these runs, their respective channel structures are also different. The count rate in the low-frequency run, for time-of-flight values above $t_D = \frac{1}{f_H}$, contains information on the energy-dependent background appearing in the high-frequency run. Calling $E(t_F)$ the neutron energy corresponding to the time-of-flight, t_F, in the high-frequency run, the associated energy background will appear in the low-frequency run at the neutron energy,

$$E^* = E(t_F + t_D) \ , \qquad (3-10)$$

where

$$\left(t_D = \frac{1}{f_H}\right) \ .$$

A program, SHIFT, was written to convert the channel structure of the low-frequency run, in the time interval $0 \leq t \leq t_D$, to the channel structure of the high-frequency run. By introducing a delay of t_D (μsec) in the SHIFT program, the TOF spectrum of the low-frequency run, in the time interval $t_D < t < 2t_D$, was displaced to the time interval, $0 \leq t \leq t_D$, and given the channel structure of the high-frequency run. Figure 9 shows the high-frequency run (upper curve) together with the tail of the low-frequency run displaced by the above procedure (lower curve). Note the presence of two broad peaks in the background. The first peak appears at 102.6 μsec and the second peak at 560 μsec. This TOF value corresponds to energies of $E^*(102.6 + t_D) = 66.0$ eV and $E^*(560 + t_D) = 37.2$ eV in the tail of the low-frequency run. Hence, these background peaks must be generated by the 36.7 (eV) and 62.02 (eV) ^{238}U resonances. Indeed the neutrons from the previous ORELA pulse, at the above resonance energies, will contribute counts appearing in the high-frequency runs as broad peaks at energies around $E(102.6) = 11$ keV and $E(560) = 396$ eV. The next two lower large ^{238}U resonances at 22 eV and 6.7 eV do not contribute because the former is outside the time range covered by the

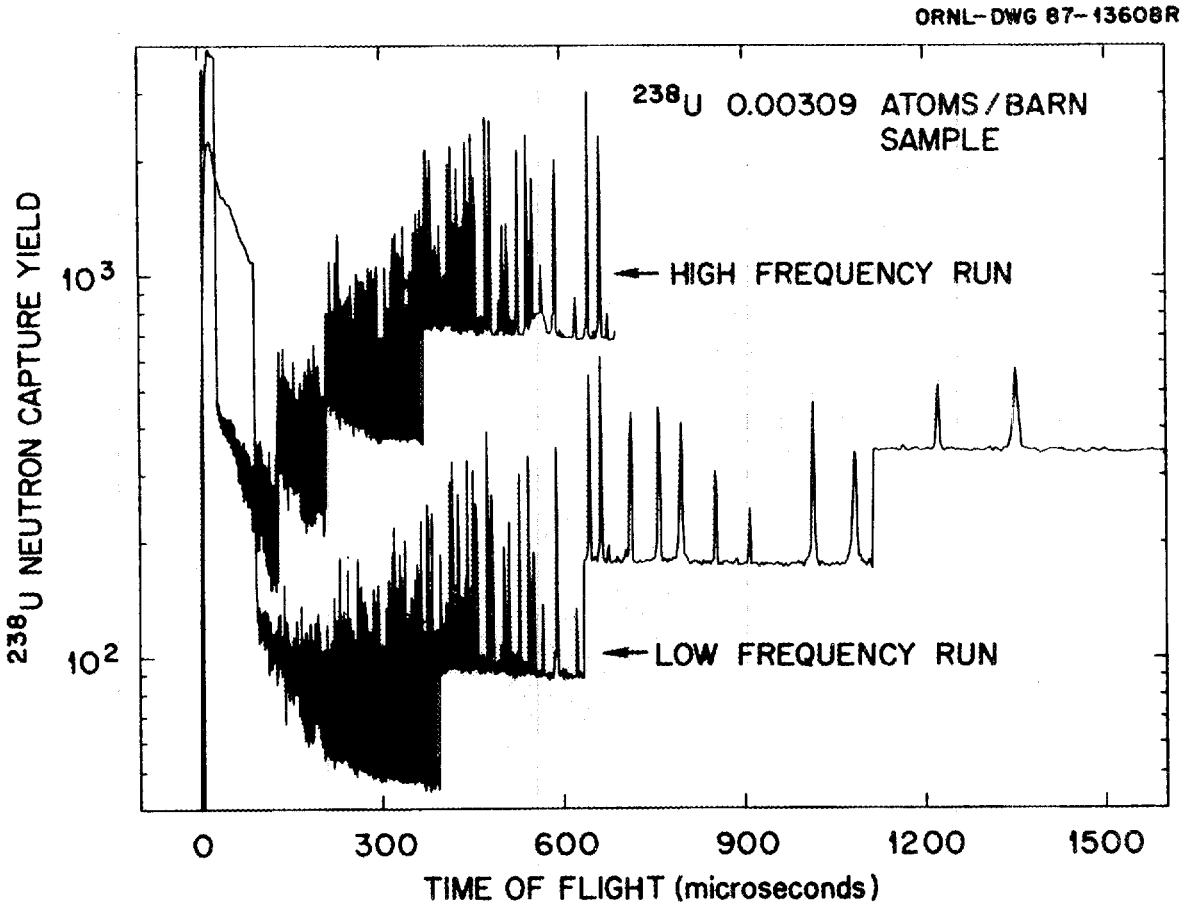

Fig. 8. Uranium-238 Capture Yield TOF Spectra Versus Neutron Time-of-Flight for the 0.00309 atoms/barn Sample. The upper trace is the TOF data for the high-frequency run, and the lower trace is the TOF data for the low-frequency run. The data shown have been averaged over 50-channel intervals. The discontinuities seen in the TOF spectra arise from changes in the channel time-width ("crunch factor").

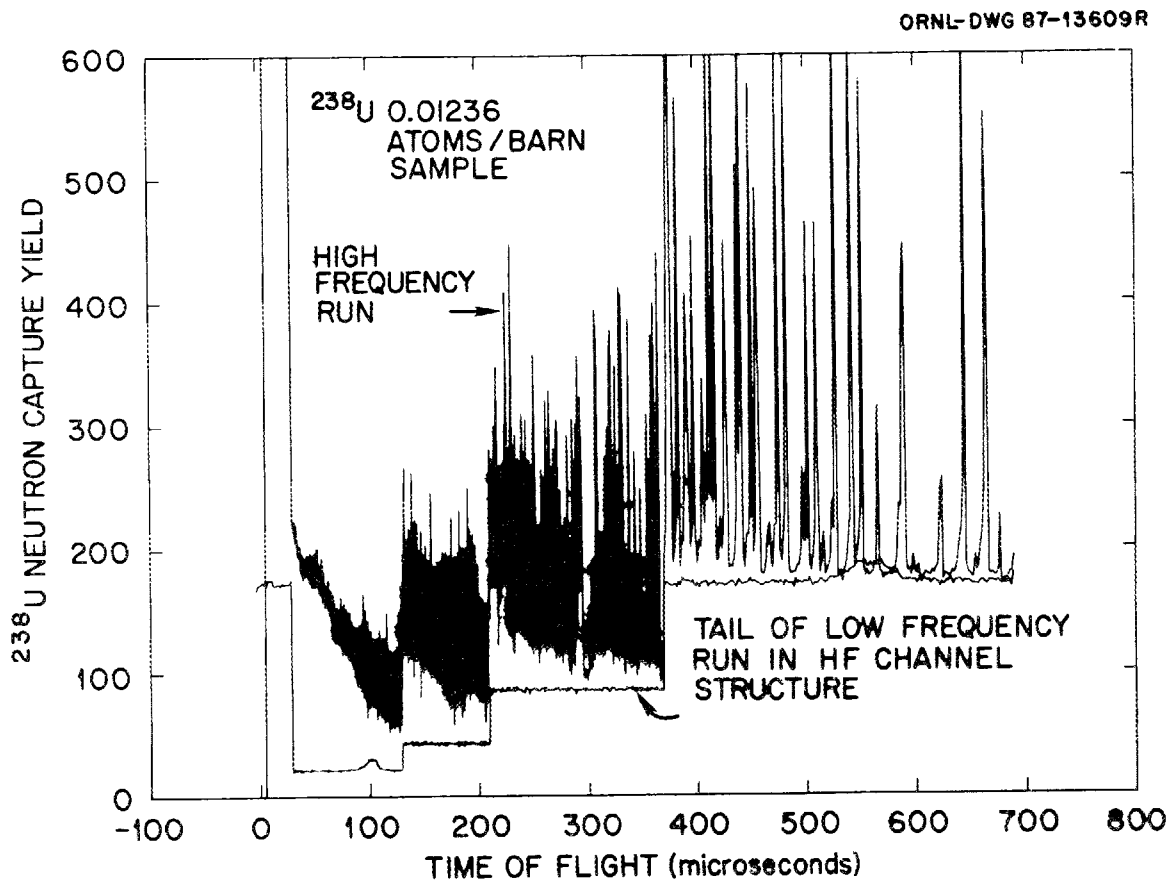

Fig. 9. Uranium-238 Capture Yield TOF Spectra Versus Neutron Time-of-Flight for the 0.01236 atoms/barn Sample. The upper trace is the TOF data for the high-frequency run. The lower trace is the overlap portion("tail") of the TOF data for the low-frequency run, which has been placed in the same channel time-width structure ("crunch") as the high-frequency run using the SHIFT program. The data shown have been averaged over 50-channel intervals. The discontinuities seen in the TOF spectra arise from changes in the channel time-width ("crunch factor").

high-frequency run and the latter corresponds to neutrons which are absorbed by the ^{10}B filter. This feature of the background, illustrated in Fig. 10, aids in the fine-tuning of the background subtraction procedure.

Calling HF_i the counts in the ith channel of the high-frequency run, one can write

$$HF_i = A_i + (B_i + B_{o_i}) \ , \qquad (3-11)$$

where

$$\begin{aligned} A_i &= \text{foreground counts,} \\ B_i &= \text{energy-dependent background counts, and} \\ B_{o_i} &= \text{constant background counts.} \end{aligned}$$

Next in the time interval, $0 < t < t_D$, we construct a TOF spectrum, TT_i, as the sum of two TOF spectra: AT_i which spans the time interval $0 < t < t_D$ in the low frequency run, and BT_i which spans the time interval, $t_D < t < 2t_D$, both spectra converted to the channel structure of the high frequency run and placed in the $0 < t < t_D$ interval. Calling A'_i the foreground counts, B'_i the energy-dependent background counts and B'_{oi}, the constant background counts of the low frequency run, we have

$$AT_i = A'_i + B'_{o_i} \qquad (3-12)$$

$$BT_i = B'_i + B'_{o_i} \ , \qquad (3-13)$$

and

$$TT_i = A'_i + B'_i + 2B'_{oi} \ . \qquad (3-14)$$

Comparing Eqs. (3-11) and (3-14) (and in view of the beam dependence of the foreground and energy-dependent background), one obtains the proportionality relation

$$A_i + B_i = a_0(A'_i + B'_i) \ , \qquad (3-15)$$

where the internormalization ratio is given by the relation

$$a_0 = X/X' \qquad (3-16)$$

with

$$X = \sum_{i=I_1}^{I_2} (A_i + B_i) \qquad (3-17)$$

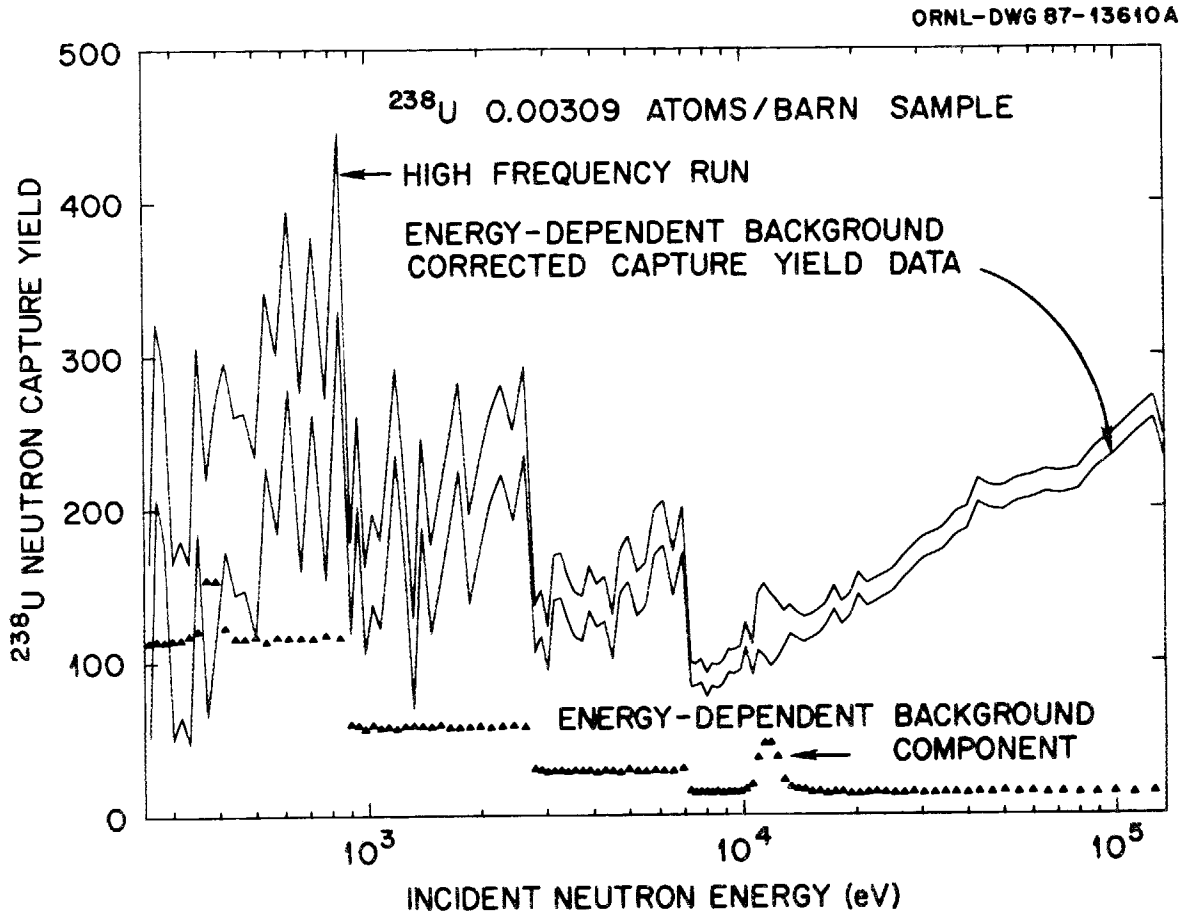

Fig. 10. Uranium-238 Capture Yield TOF Spectra Versus Neutron Energy for the 0.00309 atoms/barn Sample. The upper trace is the TOF data for the high-frequency run. The lower trace corresponds to the high-frequency run TOF data after subtraction of the energy-dependent background which is also shown. Note the broad overlap peaks at 396 eV and 11 keV. The data shown have been averaged over 50-channel intervals. The discontinuities seen in the TOF spectra arise from changes in the channel time-width ("crunch factor").

and

$$X' = \sum_{i=I_1}^{I_2} (A'_i + B'_i) \ , \qquad (3-18)$$

where I_1 and I_2 define a region in the TOF spectrum.

The ratio in Eq. (3.16) is not directly available but can be approximated by the ratio:

$$a = \frac{\sum_{i=I_1}^{I_2} HF_i}{\sum_{i=I_1}^{I_2} TT_i} = \frac{a_0 + R}{1 + R'} \qquad (3-19)$$

with

$$R = \frac{1}{X'} \sum_{i=I_1}^{I_2} B_{o_i} \quad \text{and} \quad R' = \frac{2}{X'} \sum_{i=I_1}^{I_2} B'_{o_i} \ . \qquad (3-20)$$

From the analysis of the runs with the polyetheylene plug in the beam, one concludes that the number of constant background counts per channel is a small fraction of the contributions to the count rate arising from the foreground and energy-dependent background. Hence, to a good approximation one can neglect R and R' in Eq. (3-19).

The energy-dependent background corrected TOF spectrum, EBC_i, is then obtained as

$$EBC_i = HF_i - a_o BT_i = A_i + B_{oi} \qquad (3-21)$$

3.3.2 Treatment of the Constant Background Component

Let P_i be the counts in the ith channel for the TOF spectrum measurement with the polyetheylene plug in the beam which, except for a constant, represents the constant background in the capture detector TOF spectra. To calculate the internormalization constant, b, one selects several regions between resonances in the EBC_i TOF spectrum, such that the foreground component, A_i, can be neglected. Hence making $A_i = 0$ in Eq. (3.21), the constant, b, is obtained on the ratio:

$$b = \frac{\sum_{i=I_2}^{I_3} (EBC_i)_o}{\sum_{i=I_2}^{I_3} P_i} \qquad (3-22)$$

Because of the relative smallness of the constant background, the values of P_i fluctuate considerably even though long background runs were taken. Hence, an average of the background, $< P_I >$, was taken every 1000 TOF channels, so that the constant background subtracted TOF spectrum was obtained by the relation

$$CBS_i = EBC_i - b < P_I > \tag{3-23}$$

with

$$\langle P_I \rangle = \frac{1}{1000} \sum_{i \epsilon I} P_i \tag{3-24}$$

As an illustration of the background subtraction procedure, Figure 10 shows the TOF spectra of a high-frequency run, the energy-dependent background component, and the background subtracted final result for the 2.54-mm nominal thickness ^{238}U sample, where each has been averaged over 500 TOF channels for clarity.

3.4 DETERMINATION OF THE NEUTRON BEAM SPECTRUM

The shape of the neutron beam energy spectrum, $C(E)$, is obtained from the TOF spectrum, M_i, of the neutrons detected by the ^{6}Li glass flux monitor. Several factors may affect this TOF spectrum:

1. Shape distortion arising from changing conditions at the ORELA target-moderator assembly,
2. Background contamination,
3. Multiple neutron scattering within the ^{6}Li glass, and
4. Effects of oxygen, silicon, and cerium constituents of the glass.

Shape distortion of the neutron beam spectrum at the target could result from changes in the moderator environment (such as steam bubble generation at high-power operation of the ORELA accelerator).

However, checks of the ^{6}Li glass TOF spectra for two sets of runs showed them to be consistent in the energy region considered here, as illustrated in Figure 11. The background subtraction was performed following the technique described in Section 3.3, with the exception that the internormalization constant, b, for the constant background was obtained from the count rate at the bottom of the 5.903-keV aluminum resonance dip. The effects of the cerium and silicon resonances at 1.3 keV and 56.0 keV, respectively, were eliminated by interpolating through the corresponding peaks in the neutron flux monitor TOF spectrum. The effect of the oxygen nuclei in the glass is to enhance the detector efficiency via multiple neutron

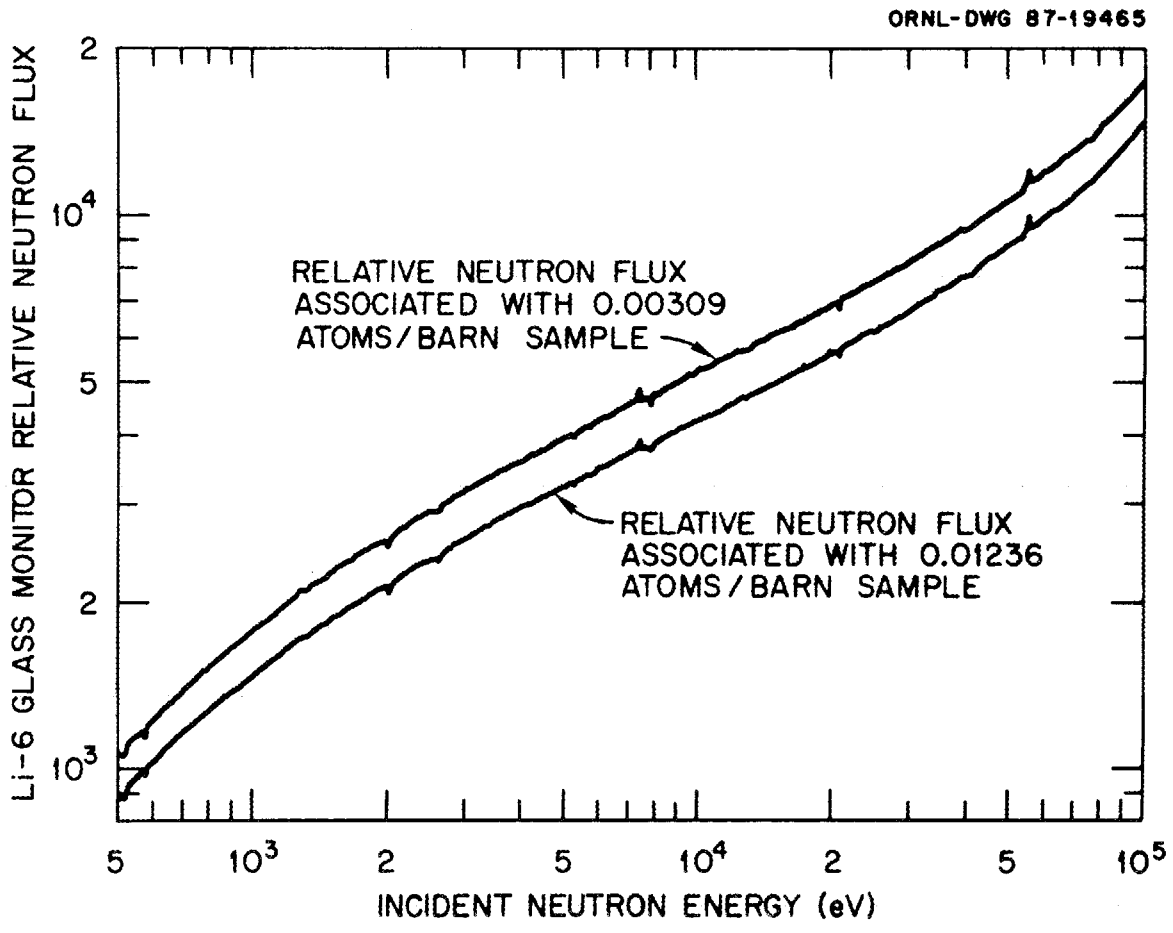

Fig. 11. Lithium-6 Glass Monitor Relative Neutron Flux Versus Incident Neutron Energy. The upper trace is the relative neutron flux associated with the 0.00309 atoms/barn sample. The lower trace is the relative neutron flux associated with the 0.01236 atoms/barn sample. The effect of the ^{28}Si resonance at 56.0 keV is clearly seen in the data. The data have been averaged over 100-channel intervals.

scattering. However, it has been shown [18] that the multiple-scattering correction is constant in the energy region between 1 keV and 100 keV, except for the effects of the cerium and silicon resonances; hence, in the energy region of interest, the multiple scattering effects do not distort the spectrum shape and can be included in the normalization factor a_n of Eq. 3-1.

The lithium glass scintillator, used as the neutron flux monitor, has a 7.7 wt % content of 95% enriched ^{6}Li as the active ingredient. At the lower end of our energy range, the neutron transmission of the lithium reduces the average efficiency of the glass about 1%. The attenuation of the neutron beam by the major constituents of the glass (silicon and oxygen) shows negligible energy dependence below 100 keV. The $^6\mathrm{Li}(n, \alpha T)$ cross section departs significantly from 1/v behavior as it nears the major p-wave resonance at 248 keV. At 100 keV, our upper limit, it is 38% above the extrapolation of the low-energy 1/v behavior.

The correction factor, $R(E)$, for the departure from the 1/v behavior can be written as

$$R(E) = \frac{1}{N\sigma_T}\left[\frac{1-T}{T}\right]F(E) \qquad (3-25)$$

where

$$N\sigma_T = \frac{\ell}{(0.34)\sqrt{E}} \text{ (dimensionless)} \qquad (3-26)$$

$$T = \exp\{-N\sigma_T\} \qquad (3-27)$$

with $\ell = 0.1$ cm (glass thickness). The factor, $F(E)$, is the ratio of the ENDF/B-VI $^6\mathrm{Li}(n, \alpha)T$ standard cross section to the 1/v cross section.[27] Figure 12 shows the energy dependence of the correction factor, R.

3.5 NORMALIZATION OF THE CAPTURE YIELD DATA

To determine the normalization constant, a_n, in Eq. 3-1, a technique proposed by Moxon[28] was utilized. This technique is based on the idea that for small resonances (i.e., with $g\Gamma_n$ small), the energy dependence of self-shielding and multiple scattering effects may be neglected. (See Appendix for further elaboration of this approximation). Hence, for these resonances, energy-dependent sample-thickness

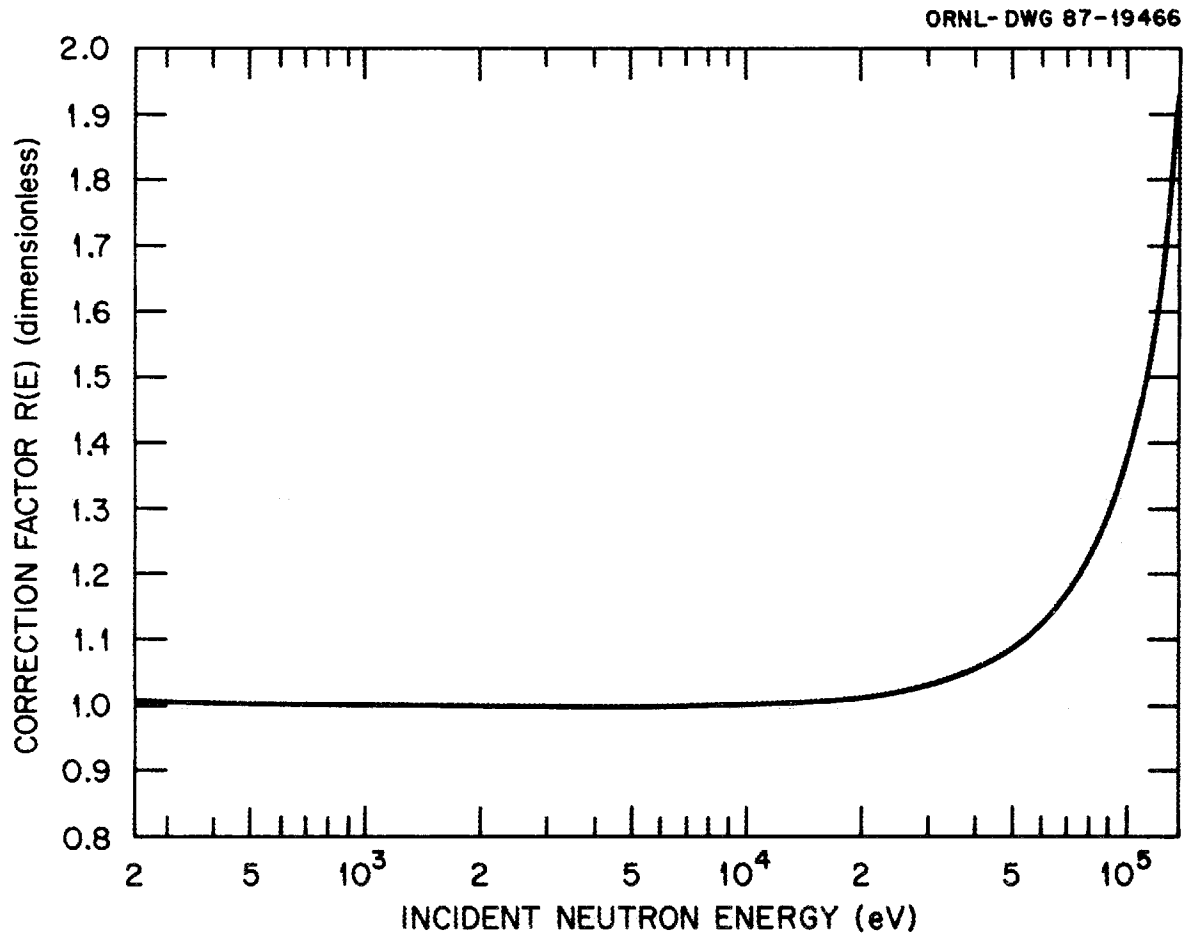

Fig. 12. The Correction Factor $R(E)$ as a Function of Incident Neutron Energy. This factor (see Equation 3-25) corrects for the reduction of Li-glass monitor efficiency due to neutron absorption by the lithium and for the departure of the ^{6}Li(n,α)T cross section from the $1v$ behavior.

effects are negligible and the capture cross section can be described by the unbroadened Breit-Wigner single-level approximation formula

$$\sigma_{n,\gamma}(E) = \frac{\pi}{k_2} \frac{g_J \Gamma_n \Gamma_\gamma}{(E - E_0)^2 + (1/2\,\Gamma)^2} \ , \qquad (3-28)$$

where

g_J	=	spin statistical factor $= \frac{(2J+1)}{2(2I+1)}$,
I	=	spin of the target nucleus,
J	=	total angular momentum,
Γ_n	=	neutron width (eV),
Γ_γ	=	capture width (eV),
E_O	=	resonance energy (eV),
Γ_T	=	total width (eV) $= \Gamma_\gamma + \Gamma_n + \Gamma_{n'}$ (eV), with
$\Gamma_{n'}$	=	inelastic neutron width (which has the value zero below the first inelastic channel at 45 keV);

and where the quantity, k, is given by [29]

$$k = k_0 E^{1/2} (\mathrm{cm}^{-1}) \qquad (3-29)$$

with

$$k_0 = 2.196771 \left[\frac{(AWR)}{(AWR+1)} \right] 10^9 \ . \qquad (3-30)$$

For the ^{238}U nucleus the Atomic Weight Ratio (AWR in Eq. 3-30 above) is 236.006. Insertion of Eq. 3-29 into Eq. 3-28 yields

$$E^{1/2} \sigma_{n,\gamma}(E) = \frac{c_0}{E^{1/2}} \frac{g_J \Gamma_n \Gamma_\gamma}{[(E - E_0)^2 + 1/4\Gamma^2]} \qquad (3-31)$$

with $c_0 = 1/k_0^2$ (cm^2).

Taking A_{TH} as the area under the Breit-Wigner resonance,

$$A_{TH} = \int_{E_1}^{E_2} dE\, E^{1/2}\, \sigma_{n_\gamma}(E) \ (\mathrm{b} \cdot \mathrm{eV}^{3/2}) \qquad (3-32)$$

and A_{EXP} as the experimental area under the unnormalized capture yield data (as defined in Eq. 3-1),

$$A_{EXP} = \int_{E_1}^{E_2} dE \left[\frac{C(E)}{S(E)} \right] R(E) \ (\mathrm{b} \cdot \mathrm{eV}^{3/2}) \ , \qquad (3-33)$$

the normalization constant, a_n, is given by the ratio

$$a_n = \frac{A_{TH}}{A_{EXP}} \ . \tag{3-34}$$

The integral in Eq. 3-32 can be calculated readily; using the change of variable

$$x = \frac{E - E_0}{1/2\Gamma_T} \tag{3-35}$$

and neglecting the energy dependence of Γ_T and Γ_n, yields

$$A_{TH} = \left(\frac{c}{E^{1/2}}\right)\left(\frac{g_J\Gamma_n\Gamma_\gamma}{\Gamma_T}\right) F(x_2, x_1) \tag{3-36}$$

with

$$F(x_2, x_1) = \frac{1}{\pi}\left[\tan^{-1}(x_2) - \tan^{-1}(x_1)\right] \ , \tag{3-37}$$

$$x_2 = \frac{E_2 - E_0}{1/2\Gamma_T} \ , \ x_1 = \frac{E_1 - E_0}{1/2\Gamma_T} \tag{3-38}$$

and

$$c = 2\pi c_0 = 4.12509^6 \ (\mathrm{b} \cdot \mathrm{eV}) \tag{3-39}$$

The values of $g_J\Gamma_n$ were obtained from the resonance data of Olsen et. al.[30] The ENDF/B-V recommended value of 0.0235 eV was used for the capture width, Γ_γ, for all the small resonances used in the calculation of the normalization constants.

Previous work at ORNL concerning the measurement of gamma-ray intensities[31] showed that for both Breit-Wigner and Gaussian line shapes which are contaminated with background noise, a nearly optimal estimation of the area under the curve is obtained using the limits of integration

$$E_1 = E_0 - 1/2\,\Delta E(1/5) \tag{3-40}$$

and

$$E_2 = E_0 + 1/2\,\Delta E(1/5) \ , \tag{3-41}$$

where $\Delta E(1/5)$ is the full width (eV) at one-fifth (1/5) of the maximum amplitude.

Table VII shows the normalization constant calculations for the TOF spectra for the 0.01236 atoms/barn and 0.00309 atoms/barn ^{238}U samples, respectively. The normalization constants were taken to be the simple arithmetic means for each

sample, i.e.,: $a_n = 64.7 \pm 4.0$ for the 0.01236 atoms/barn sample and 191.9 ± 15.0 for the 0.00309 atoms/barn sample. (See Section 3.6) for the assigned uncertainties).

Table VII. Normalization Constants for the 0.01236 and 0.00309 atoms/barn ^{238}U Samples, as Calculated from Various Small ^{238}U Resonances by the Moxon Technique

E_0 (eV)	$g\Gamma_n{}^a$ (meV)	$a_n{}^{b,d}$	$a_n{}^{c,d}$
624.20 ± .07	.82 ± .09[a]	67.33	171.02
677.75 ± .10	.66 ± .10	59.66	190.62
756.24 ± .14	.55 ± .10	65.33	180.53
808.16 ± .21	.44 ± .10	59.16	223.17
846.65 ± .11	.87 ± .13	65.76	176.30
891.23 ± .08	.77 ± .09	66.80	216.07
977.37 ± .10	.77 ± .11	62.94	177.15
1062.68 ± .13	.96 ± .17	70.85	200.59
		64.7 ± 4.0[e]	191.9 ± 15.0[e]

[a]The listed uncertainties are statistical only. There is in addition a systematic uncertainty of 3% (Olsen et al., ref. 30).

[b]0.01236 atoms/barn sample.

[c]0.00309 atoms/barn sample.

[d]The radiation width was taken to be the ENDF/B-V recommended value of 23.5 MeV.

[e]The ratio of these averages is less than the ratio of sample thicknesses (i.e., 4.0) because of gamma ray and neutron energy losses within each sample.

3.6 UNCERTAINTIES IN THE MEASUREMENTS

Two types of uncertainties must be considered: the statistical counting uncertainty, which is uncorrelated between time-of-flight channels, and the correlated systematic uncertainties.

The statistical uncertainty for each sample was obtained by systematically following the propagation of the standard deviation of Poisson distributed statistical

samples, at each step in the data reduction process. The relative error in the ith channel of the capture yield TOF spectrum is then given by the relation

$$\frac{\delta Y_c(i)}{Y_c(i)} = \frac{[HF(i) + a\,BT(i)]^{1/2}}{CBS(i)} \quad , \qquad (3-42)$$

where the symbols on the right hand side of in Eq. 3-42 have been previously defined in Section 3.3.1.

The main sources of systematic uncertainties are the background subtraction uncertainties in the TOF spectra for the ^{238}U counts in the ORELAST and the neutron monitor counts, and normalization uncertainties. To estimate the uncertainties associated with the background subtraction procedure, the sensitivity coefficients, S_i, below were computed for each channel, i, in the TOF spectra.

$$S_i = \frac{a}{Y_c(i)} \frac{\Delta Y_c(i)}{\Delta a} \quad , \qquad (3-43)$$

where

$\Delta a/a$	=	percent change in the background subtraction constant,
$\Delta Y_c(i)/Y_c(i)$	=	percent change in the capture yield, and
$\Delta Y_c(i)$	=	change in the capture yield upon a change Δa in the background subtraction constant.

The sensitivity coefficients were computed for the energy-dependent and constant background subtractions for both the ORELAST and ^{6}Li glass neutron monitor TOF spectra. These calculations were carried out by changing the energy-dependent background subtraction constant (or the constant background subtraction constant) by 5% and proceeding through all the sequence of steps in the data reduction process with no other changes.

The background subtraction uncertainties (from both the energy-dependent and constant background contributions) were obtained by the convolution of the sensitivity coefficients, with the estimated uncertainties in the constant, a, for each of the background subtraction procedures. These uncertainties were then combined to yield r.m.s. estimates of the systematic uncertainties arising from the background subtraction procedure. Following this procedure, the uncertainties were estimated to be about 5% up to 10 keV and 4% from 10 keV up to 100 keV.

The uncertainties in the normalization constant, a_n, arise from several sources: (a) the determination of the experimental area, A_{EXP}; (b) uncertainties in the resonance parameters, and (c) neglect of sample thickness effects. The uncertainty in the calculation of the areas under the resonances chosen for the normalization procedure, was estimated to be about 3%. The contribution to the overall uncertainty, arising from the uncertainty in the resonance parameters, is mostly due to the statistical uncertainties in the determination of the neutron widths, since the areas of the small resonances used in the normalization procedure are quite insensitive to the radiation width values. A 3% systematic uncertainty (see Appendix A) was assigned to the normalization constant, arising from the neglect of sample thickness effects. The combination of these uncertainties, produced a r.m.s. normalization error of 6% for the 0.01236 atoms/barn sample and 8% for the 0.00309 atoms/barn sample. Since a large fraction of the normalization uncertainty arises from the statistical uncertainties in the determination of the neutron widths, it is hoped that new ORELA high neutron energy resolution transmission measurements[32] (in progress) may yield more accurate estimates for the neutron widths of the small ^{238}U resonances.

4. RESULTS AND DISCUSSION

Our (normalized) capture yield data averaged over decimal energy intervals between 0.3 keV and 100 keV are shown in Table VIII for the 0.01236 atoms/barn and 0.00309 atoms/barn samples.

The capture yield is related to the resolution-broadened and Doppler-broadened neutron capture cross section $\sigma_{n.\gamma}(E)$, by the relation

$$Y_c(E) = \bar{\sigma}_{n\gamma}(E) S_s(E,N) M_s(E,N) \qquad (4-1)$$

where

$$S_s(E,N) = \text{self} - \text{shielding factor} = [1 - \exp\{-N\sigma_T(E)\}]/N\sigma_T(E) \qquad (4-2)$$

and

$$M_s(E,N) = \text{multiple scattering factor} = \left[1 - \frac{\bar{\sigma}_{n\gamma}(E)}{\sigma_T(E)} P_c(N,E)\right]^{-1} \qquad (4-3)$$

with

$$\begin{aligned} N &= \text{sample thickness (atoms/barn)}, \\ \sigma_T(E) &= \text{total neutron cross section, and} \\ P_c(N,E) &= \text{mean collision probability } (P_c(0,E) = 0). \qquad (4-4) \end{aligned}$$

Note that it is only for infinitely thin samples (i.e., $N \rightarrow 0$), that $S_s(0,E)$ and $M_s(0,E)$ become unity and there is equivalence between capture cross section and capture yield.

Capture data for the two ^{238}U samples used in the present measurements are shown in Figure 13 for neutron energies in the resolved resonance region. These results clearly show substantial sample thickness effects in the large resonances. Figure 14 displays capture yield data for the two samples in the neutron-energy range 25 to 100 keV, where the data in each case have been averaged over 250 time-of-flight channels. Note that in the region from 25 up to 50 keV, there appears to be a considerable cancellation between the self-shielding and multiple scattering effects for the two sample thicknesses.

Table VIII. Capture Yield Over Decimal Energy Intervals from 0.3 keV up to 100 keV for the 0.01236 atoms/barns and 0.00309 atoms/barn Samples

ΔE (keV)	Y_c[a] (0.01236 atoms/b)	Y_c[a] (0.00309 atoms/b)
.3 – 0.4	1.15 ± .06	1.87 ± .09
.4 – 0.5	1.91 ± .10	2.52 ± .13
.5 – 0.6	1.89 ± .09	3.46 ± .17
.6 – 0.7	1.84 ± .09	2.81 ± .14
.7 – 0.8	2.61 ± .08	1.88 ± .09
.8 – 0.9	1.67 ± .08	2.47 ± .12
.9 – 1.	1.88 ± .09	2.95 ± .15
1. – 2.	1.31 ± .07	1.73 ± .09
2. – 3.	1.15 ± .06	1.37 ± .07
3. – 4.	1.08 ± .05	1.21 ± .06
4. – 5.	.907 ± .045	.962 ± .048
5. – 6.	.899 ± .045	.947 ± .047
6. – 7.	.852 ± .043	.905 ± .045
7. – 8.	.794 ± .040	.814 ± .041
8. – 9.	.678 ± .034	.708 ± .035
9. – 10.	.727 ± .036	.743 ± .037
10. – 20.	.629 ± .030	.641 ± .026
20. – 30.	.503 ± .020	.505 ± .020
30. – 40.	.440 ± .018	.443 ± .018
40. – 50.	.392 ± .016	.396 ± .016
50. – 60.	.324 ± .013	.336 ± .013
60. – 70.	.283 ± .011	.294 ± .012
70. – 80.	.243 ± .009	.264 ± .011
80. – 90.	.223 ± .009	.239 ± .009
90. – 100.	.214 ± .009	.229 ± .009

[a]Normalization uncertainties not included.

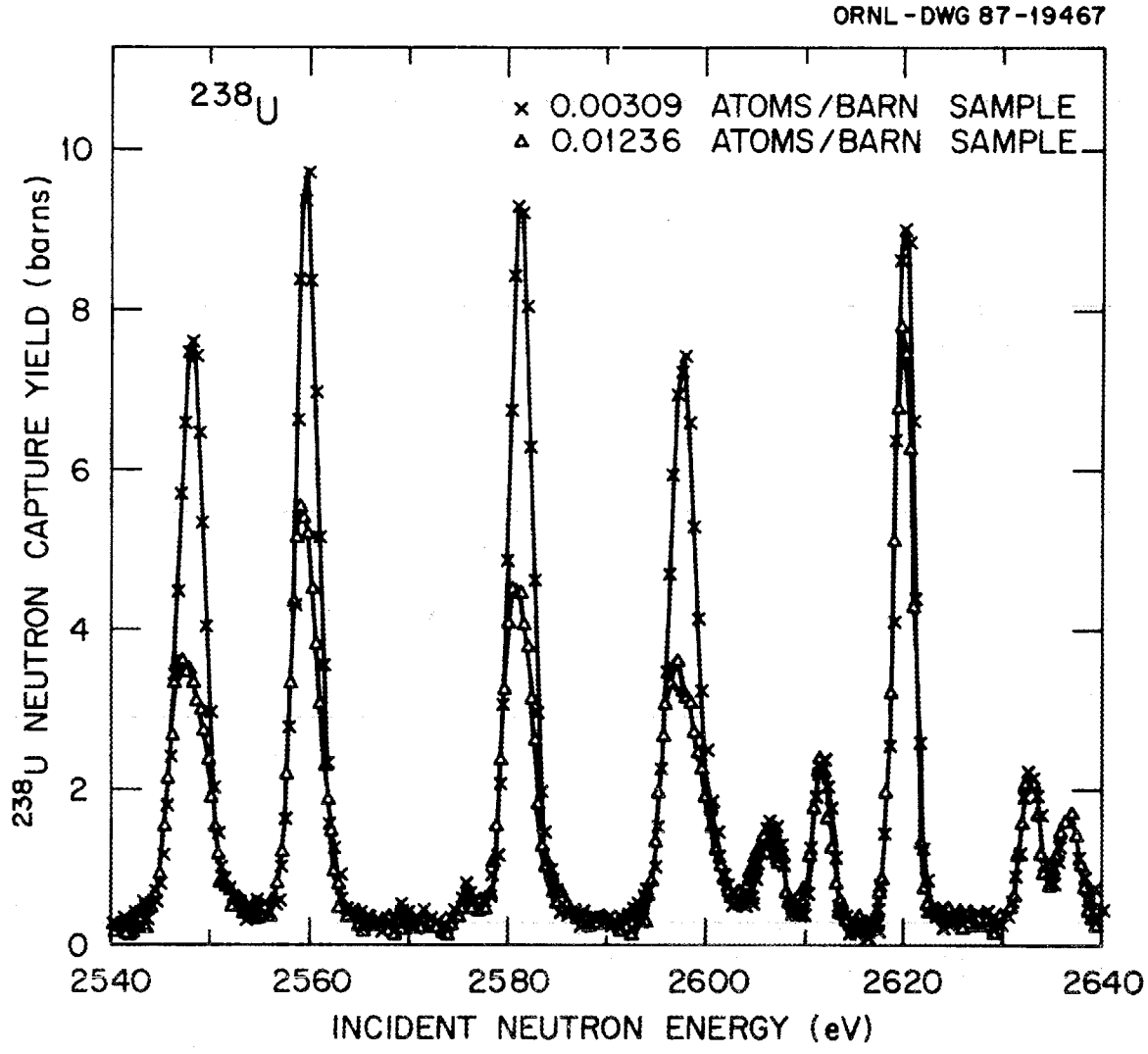

Fig. 13. Capture Yield Data for the 0.00309 atoms/barn and 0.01236 atoms/barn Samples in the Neutron Energy Range from 2540 eV to 2640 eV. The lines shown merely connect the data symbols for each sample for clarity. Note the appearance of substantial sample thickness effects on the larger resonances.

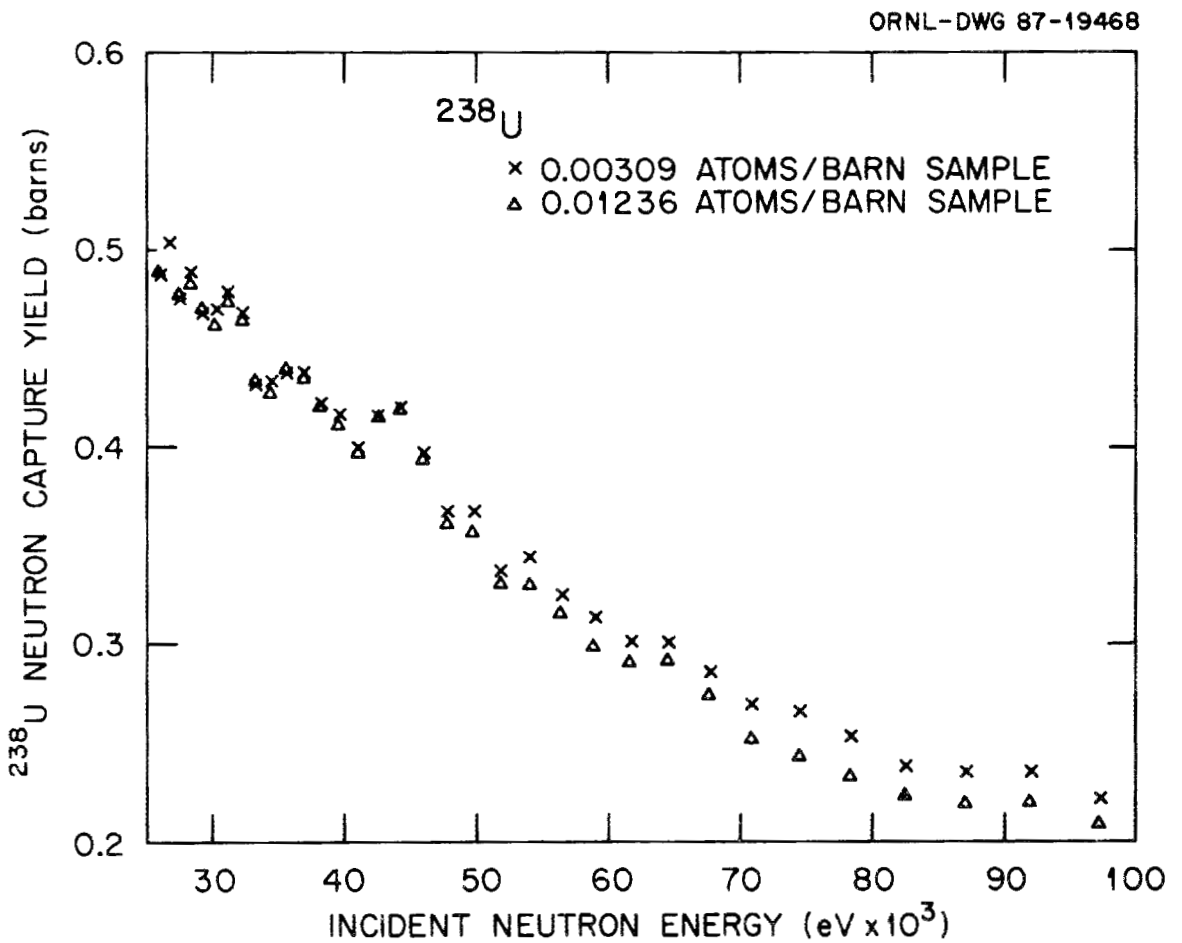

Fig. 14. Capture Yield Data for the 0.00309 atoms/barn and 0.01236 atoms/barn Samples in the Neutron Energy Range from 25 keV to 100 keV. The data have been averaged over 250-channel intervals. Note the cancellation between self-shielding and multiple scattering effects in the energy region from 25 keV to 50 keV.

The high-energy resolution achieved in the present work is illustrated in Figures 15 and 16 which show examples of the capture yield data around 15 keV and 23 keV, respectively, for the 0.01236 atoms/barn sample. The energy resolution of these data will allow the possibility of extending the evaluated resolved resonance energy region for ^{238}U beyond its current 4-keV limit. Above 20 keV the present data exhibit a substantial amount of intermediate structure in the capture yield. This is illustrated in Figures 17, 18, and 19 which show capture yield data for the two ^{238}U samples in the energy regions covering 30 to 40 keV, 40 to 50 keV, and 50 to 90 keV, respectively. These data, which have been averaged over one hundred or fifty time-of-flight channels to eliminate statistical fluctuations, show a remarkable amount of intermediate structure which appears extremely consistent in both samples. The existence of this intermediate structure in the ^{238}U neutron capture yield is of importance for the calculation of self-shielded neutron group cross sections and for the determination of the Doppler coefficient of reactivity. Figure 20 shows the ^{238}U neutron capture cross section between 10 keV and 100 keV as prescribed by the ENDF/B-V evaluation,[33] with the capture yield data for the 0.00309 atoms/barn samples in the present work superimposed. It appears that the ENDF/B-V evaluation does not provide the amount of intermediate structure observed in the measurement.

An interesting result of the present work has been the discovery of many small resonances of the (^{238}U + n) compound nucleus which have not been detected in previous capture or transmission measurements. In addition, multiple splittings of what appeared to be single resonances in previous measurements have been observed. Table IX presents a listing of resonance energies for some 200 resonances which were not seen in the high-resolution transmission measurement of Olsen et al.[13,30] at 150 m in the energy range from 250 eV to 10 keV.

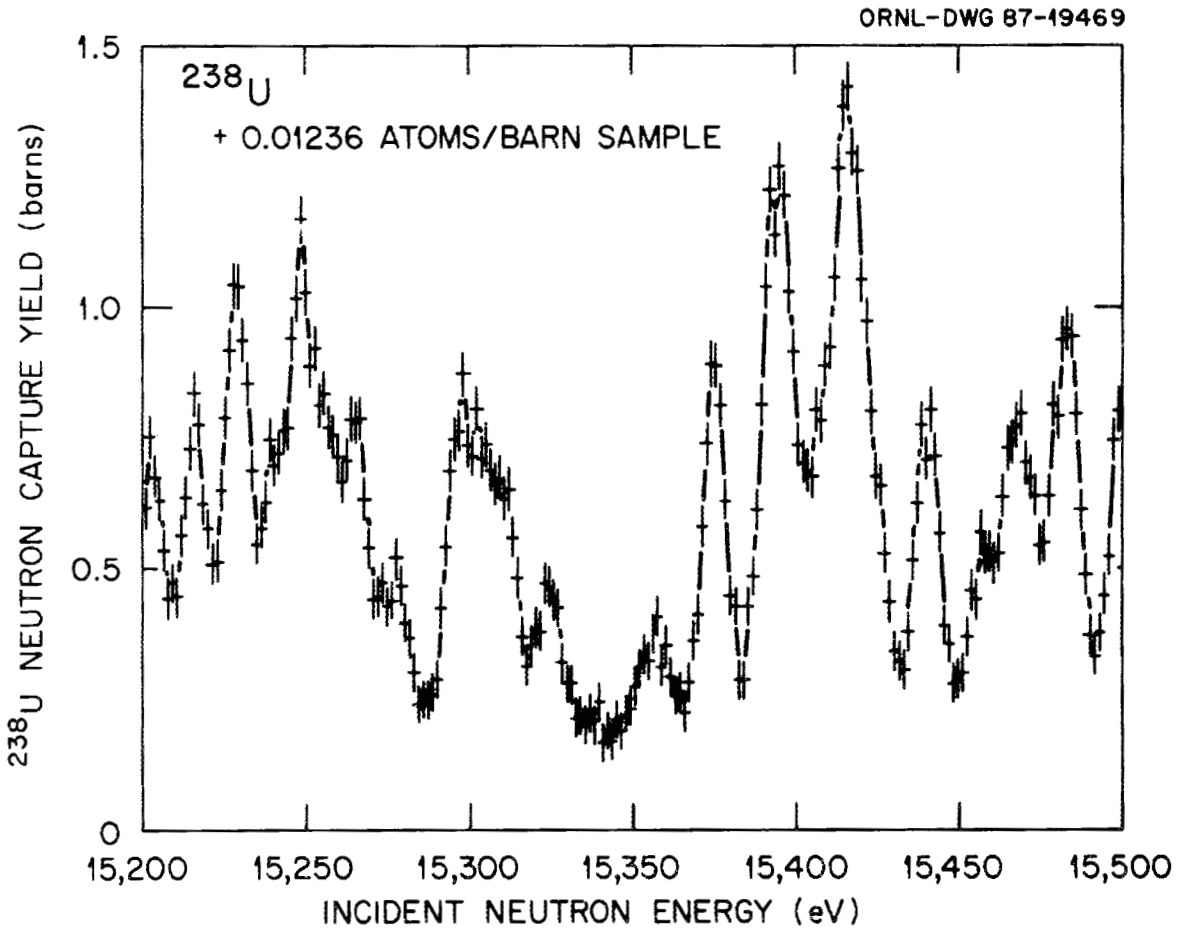

Fig. 15. Capture Yield Data in the Neutron Energy Range from 15.2 keV to 15.5 keV for the 0.01236 atoms/barn Sample. Note the high resolution achieved by the present measurement which is a factor of three better than any previous measurement in this energy region. The vertical bars indicate statistical uncertainties only.

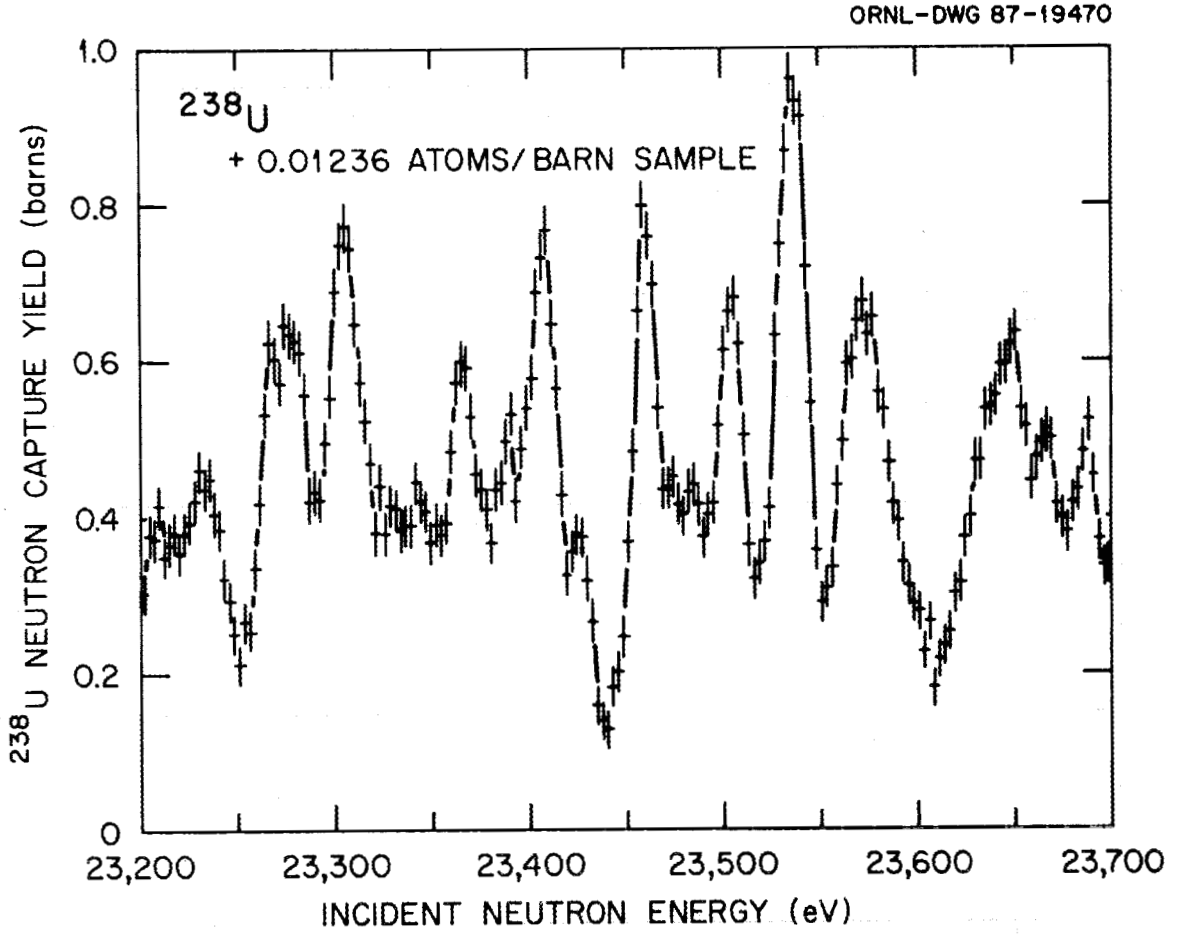

Fig. 16. Capture Yield Data in the Neutron Energy Range from 23.2 keV to 23.7 keV for the 0.01236 atoms/barn Sample. Note the high resolution achieved by the present measurement which is a factor of three better than any previous measurement in this energy region. The vertical bars indicate statistical uncertainties only.

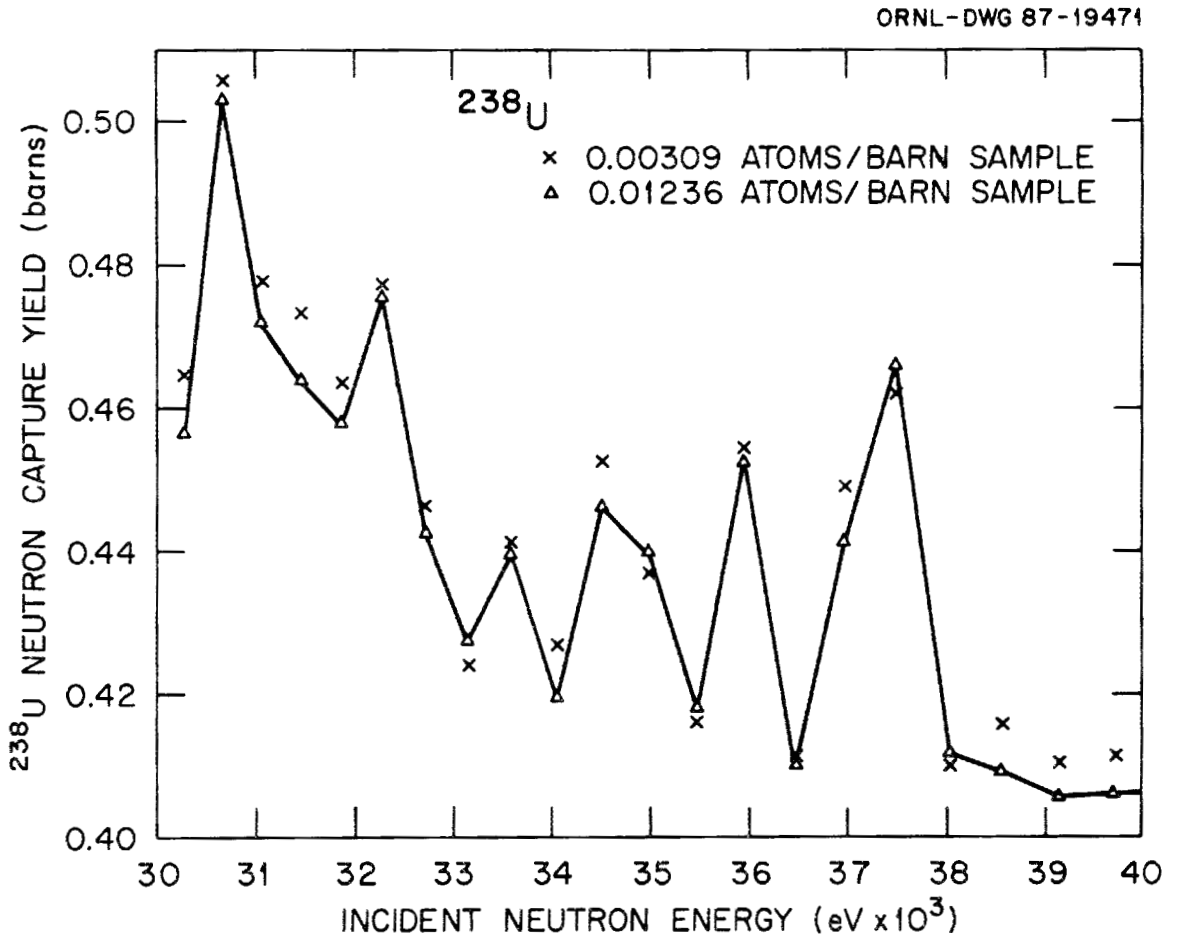

Fig. 17. Capture Yield Data for the 0.00309 atoms/barn and 0.01236 atoms/barn Samples in the Neutron Energy Range from 30 keV to 40 keV. The data have been averaged over 100-channel intervals. Note the good reproducibility of the observed intermediate structure between the two samples.

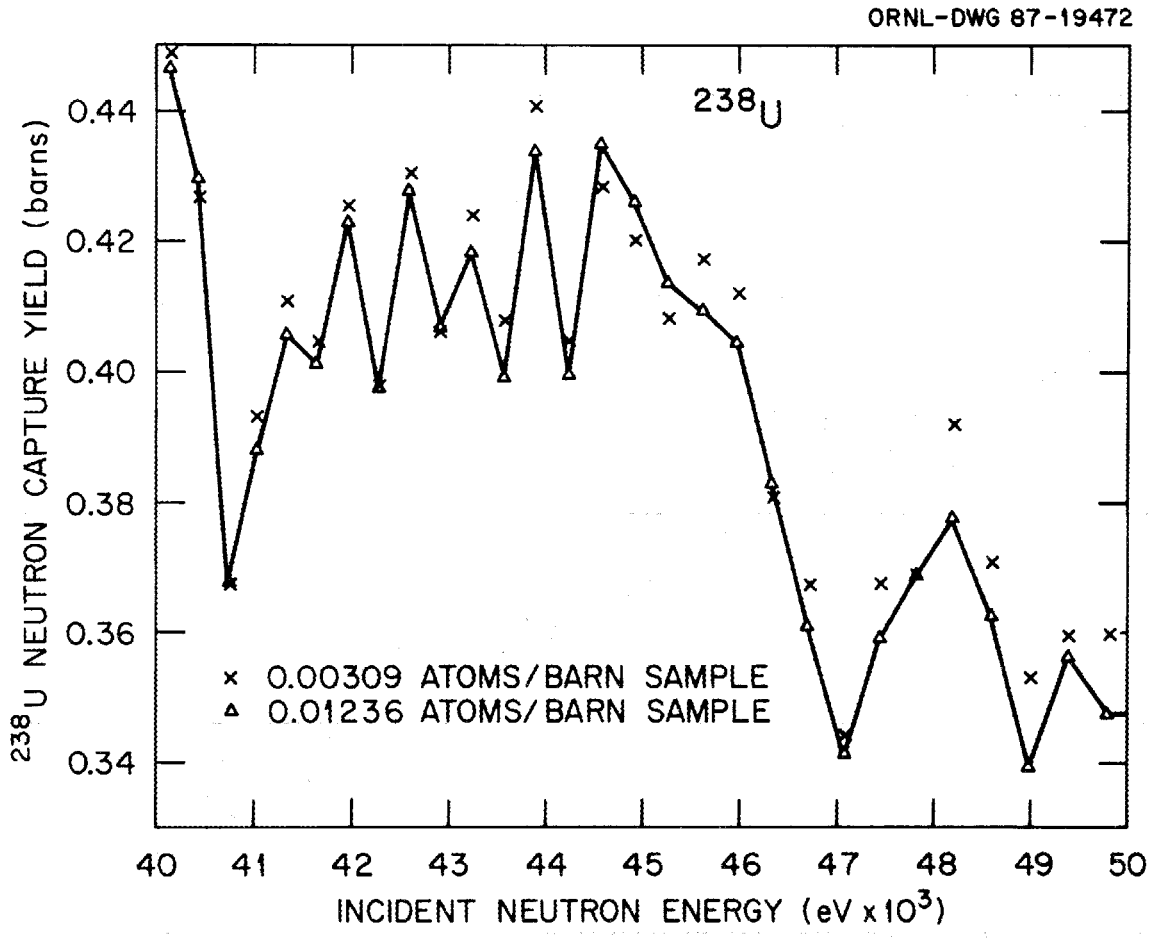

Fig. 18. Capture Yield Data for the 0.00309 atoms/barn and 0.01236 atoms/barn Samples in the Neutron Energy Range from 40 keV to 50 keV. The data have been averaged over 50-channel intervals. Note the good reproducibility of the observed intermediate structure between the two samples.

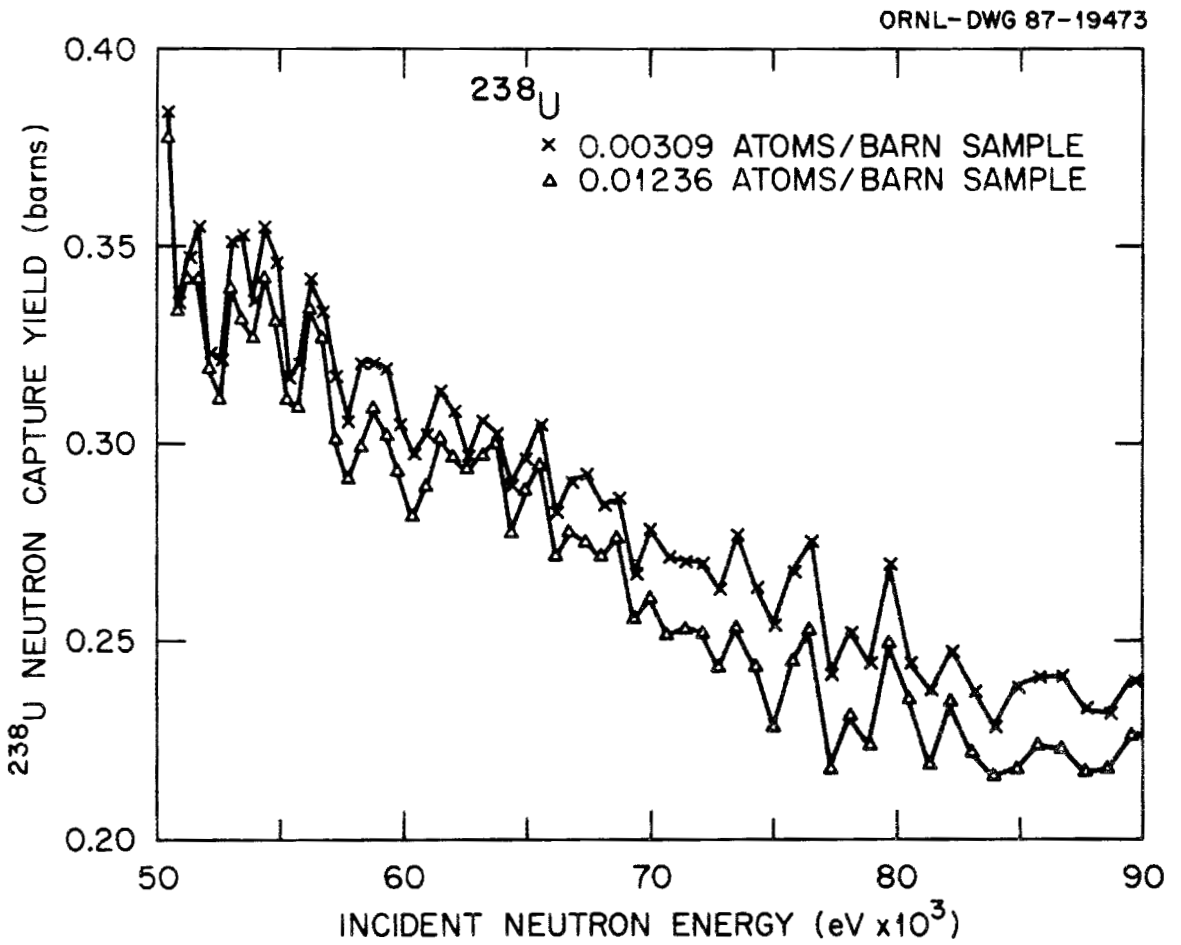

Fig. 19. Capture Yield Data for the 0.00309 atoms/barn and 0.01236 atoms/barn Samples in the Neutron Energy Range from 50 keV to 90 keV. The data have been averaged over 50-channel intervals. Note the good reproducibility of the observed intermediate structure between the two samples.

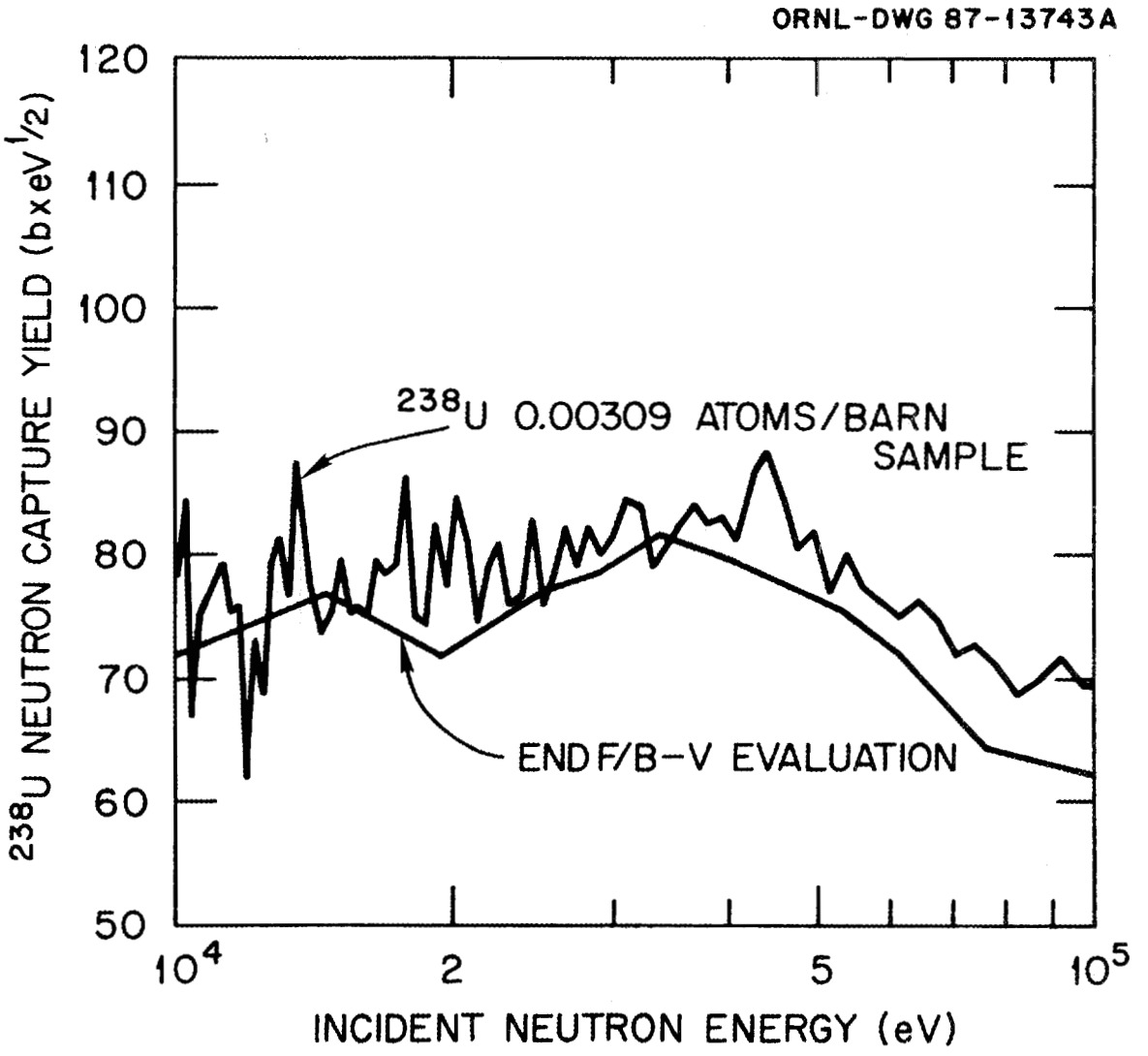

Fig. 20. Comparison of the Intermediate Structure Observed in the Capture Yield Data for the 0.00309 atoms/barn Sample with the Structure Introduced in the ^{238}U Capture Cross Section by the ENDF/B-V Evaluation (Reference 33) in the Neutron Energy Range from 10 keV to 100 keV. The data have been averaged over 250-channel intervals. Because of the lack of sample thickness corrections in the capture yield data, the present comparison is only intended to be of a qualitative nature.

Table IX. List of Resonances (250 eV to 10 keV) Not Detected in Previous ^{238}U Transmission Measurement[13] at 150 Meters

Energy (eV)	Energy (eV)	Energy (eV)	Energy (eV)	Energy (eV)	Energy (eV)
734.9	2825.3	4497.6	5703.7	7515.1	8973.2
770.6	2846.4	4529.9	5727.8	7530.1	8978.2
772.3	3048.5	4551.6	5907.6	7583.7	8994.2
800.9	3157.6	4573.5	5910.8	7631.8	9056.0
834.2	3210.2	4602.7	6102.4	7707.8	9111.8
907.2	3214.9	4677.1	6334.0	7714.9	9121.8
982.0	3233.0	4716.0	6369.5	7740.0	9123.8
984.2	3257.8	4775.9	6466.0	7745.9	9183.0
1278.5	3413.6	4812.5	6530.1	7793.3	9193.9
1456.4	3447.4	4839.6	6557.9	7795.3	9195.3
1492.2	3471.1	4870.8	6559.8	7820.0	9204.2
1562.6	3506.7	4961.1	6601.0	7865.1	9207.5
1577.6	3542.1	5063.8	6603.7	7892.4	9224.8
1614.1	3547.2	5067.1	6617.8	7917.3[a]	9228.0
1766.6	3584.0	5095.9	6621.5	8018.6	9291.8
1985.4	3603.5	5110.3	6672.6	8059.3	9311.4
2035.2	3746.5	5128.7	6717.6	8066.7	9339.3
2038.4	3791.1	5150.1	6719.4	8078.0	9344.5
2063.6	3809.1	5152.2	6730.0	8122.7	9516.8
2126.0	3949.5	5177.7	6732.0	8168.7	9540.5
2140.5	3962.4	5180.4	6754.0	8171.6	9567.7
2179.0	3974.8	5327.5	6768.2	8233.3	9716.7
2192.5	3979.5	5329.2	6775.9	8268.0	9721.0
2197.3	3993.2	5330.8	6778.3	8295.9	9783.3
2219.9	4052.3	5441.1	6941.4	8303.1	9784.7
2304.9	4100.9	5443.8	6989.6	8342.2	9810.9
2434.9	4104.9	5567.6	6993.0	8343.8	9813.7
2439.4	4158.1	5569.2	7055.4[a]	8427.7	9821.6

Table IX. Continued

Energy (eV)	Energy (eV)	Energy (eV)	Energy (eV)	Energy (eV)	Energy (eV)
2452.3	4182.9	5570.5	7076.4	8439.2	9876.3
2468.0	4202.5	5597.6	7110.1[a]	8442.2	9878.5
2509.5	4236.3	5598.9	7226.2	8520.6	9888.0
2534.5	4245.0	5601.7	7332.8	8621.3	9890.3
2575.8	4270.4	5632.3	7352.4	8643.9	9920.0[a]
2647.4	4319.5	5635.3	7382.6	8680.1	9938.5[a]
2654.4	4341.1	5658.2	7387.0	8697.4	9959.9
2688.1	4413.3	5664.1	7469.0	8717.7[a]	9979.3
2720.5	4426.8	5688.8	7477.0	8796.2	
2732.8	4439.8	5690.6	7490.1	8798.5	
2779.1	4441.7	5702.1	7512.2	8811.1	

[a]Possible doublet or multiple.

5. SUMMARY AND DISCUSSION

A high neutron energy resolution measurement of the ^{238}U neutron capture yield has been performed using the Oak Ridge Electron Linear Accelerator (ORELA) as the pulsed neutron source.

A technique has been developed for the estimation of the energy-dependent background, which is based on the measurement of the neutron pulse overlap, by performing measurements of the time-of-flight (TOF) spectra at different ORELA pulse rates.

A careful analysis has been performed of the pulse-height distribution of the gamma-ray detector (ORELAST) counts, with the purpose of ascertaining the effect of the energy dependence of the gamma-ray cascades and of possible electronic bias shifts at the ORELAST on the TOF spectra. To this end, the pulse-height spectrum was divided into five bins, and each one of the TOF spectra was separately analyzed. It was found that the different signal-to-background ratios exhibited by the TOF spectra in each pulse-height bin were sufficient to explain the discrepancies among the TOF spectra corresponding to the various pulse-height bins. Hence, any effect of gamma-ray cascade changes with neutron energy, resonance spin and parity, or of electronic bias shifts are probably masked by the uncertainties associated with the background subtraction process.

The normalization of the present data must be taken as preliminary, pending a simultaneous resonance analysis of transmission data and the present capture data.

No attempt has been made to correct the present capture yield data for sample thickness effects. Such correction (necessary to derive capture cross section) would require a consistent set of resonance parameters, which are not yet available, for both the resolved and unresolved resonance energy regions. In the past, sample thickness corrections have been performed with inconsistent parameter sets and approximate calculational algorithms which introduced additional uncertainties to the data. These uncertainties resulted in a situation where the discrepancies among various sets of ^{238}U neutron capture measurements were larger than their quoted experimental uncertainties.[9] In view of this, it was concluded that the neutron cross-section technology community would be better served by providing high energy resolution capture yield data for two largely different sample thicknesses. These data can then be used as a testing ground for resonance parameter sets and calculational

algorithms now in use for reactor design. In this regard, the present data have been released to (and are currently in use by) both the ^{238}U International Task Force and the National Nuclear Data Center at Brookhaven National Laboratory.

Some 200 small resonances of the (^{238}U + n) compound nucleus have been observed which had not been detected in transmission measurements, in the energy range from 250 eV to 10 keV. These results will allow the development of improved resonance parameter sets, particularly when combined with high resolution ^{238}U transmission measurements currently in progress at ORELA.

The high energy resolution achieved in this measurement in several cases resulted in doublet and triplet splittings of what appeared to be single resonances in previous measurements. This resolution should allow extension of the evaluated resolved resonance energy region in ^{238}U from the present 4-keV limit up to 15- or 20-keV incident neutron energy.

A substantial amount of intermediate structure has been detected above 20 keV which is very well reproduced in the capture yield measurements of two largely different sample thicknesses of ^{238}U. Addition of this intermediate structure to future generations of the ENDF/B evaluations should allow improved calculation of self-shielded group cross sections and Doppler coefficients of reactivity, which are important parameters for the design of both thermal and fast fission reactors, as well as possible "blanketed" fusion reactors of the future.

6. APPENDIX A

6.1 SAMPLE THICKNESS CORRECTIONS FOR WEAK CAPTURE RESONANCES IN ^{238}U IN THE NORMALIZATION REGION (600 EV - 1100 EV)

This appendix elaborates on the neglect of sample size corrections in the calculation of the normalization constant (see Section 3.5). For weak capture resonances (i.e., $g\Gamma_n << \Gamma_\gamma$), the capture probability is proportional to the neutron width. Hence the probability of capturing those neutrons which reached the resonance energy after several collisions in the sample is indeed very small. Thus, it appears justifiable to neglect multiple scattering corrections in weak capture resonances. The self-shielding factor, S_S, (see Eq. 4-2) is large even for small resonances, due to the potential cross-section contribution, σ_p, to the total neutron cross section, $\sigma_T(E)$. However, the potential cross section is nearly constant over a large neutron-energy range, and its contribution to the resonance self-shielding can be included in the normalization constant.

By writing

$$\sigma_T(E) = \sigma_p + \sigma_c(E) \qquad (A-1)$$

where

$\sigma_c(E)$ = capture cross section (eV),

the expression for the self-shielding factor can be rewritten in the form

$$\frac{S_S}{S_{S_p}} = \left(1 + \frac{<\sigma_c>}{\sigma_p}\right)^{-1} + \frac{e^{-N\sigma_p}}{S_{S_p}} \left[\frac{<\sigma_c>/\sigma_p}{1+\frac{<\sigma_c>}{\sigma_p}}\right] \qquad (A-2)$$

where

N = sample areal density (atoms/barn)

and the self-shielding factor for potential scattering is given by

$$S_{S_p} = \frac{(1 - e^{-N\sigma_p})}{N\sigma_p} \qquad (A-3)$$

In Eq. A-2, one must also define $<\sigma_c>$ = average capture cross section over the ^{238}U resonance and make the approximation (for $N\sigma_c << 1$) that

$$e^{-N<\sigma_c>} = 1 - N<\sigma_c> \qquad (A-4)$$

For a ^{238}U capture resonance with $g\Gamma_n = 1.06$ meV and $\Gamma_\gamma = 23.6$ meV, the value $< \sigma_c >$, calculated as half the peak cross section is equal to 3.605 barns. With a value of $\sigma_p = 9.38$ barns for the ^{238}U nucleus, one obtains the following values for the ratio of the overall self-shielding factor, S_S, to the potential scattering self-shielding factor, S_{S_p}:

1. Thick sample ($N = 0.01236$ atoms/barn)

$$\frac{S_S}{S_{S_p}} = 0.984$$

   and

2. Thin sample ($N = 0.00309$ atoms/barn)

$$\frac{S_S}{S_{S_p}} = 0.996 \ .$$

   Thus, the energy-dependent part of the self-shielding factor is less than 2% for the thick sample and only a fraction of 1% for the thin sample. In fact, these corrections are upper bounds, as the range of neutron widths for the particular set of resonances used in the normalization procedure (see Table VII) was from 0.44 to 0.96 meV.

REFERENCES

1. W. P. Poenitz, *Proceedings of Specialists Meeting on Fast Neutron Capture Cross Sections*, ANL-83-4 (1983), p. 288.
2. WRENDA 83/84, INDC(SEC)-88/URSF (1983).
3. M. Sowerby, "Summary of the Work of the NEANDC Task Force on U-238," *Int. Conf. on Nuclear Data for Basic and Applied Science, May 13-17, 1985, Santa Fe, N.M.*
4. G. de Saussure, E. G. Silver, R. B. Perez, R. Ingle, H. Weaver, *Nucl. Sci. and Eng.*, 5 385 (1973).
5. M. C. Moxon, AERE-R 6074 (1969).
6. M. P. Fricke, W. M. Lopez, S. J. Friesenhahn, A. D. Carlson, and D. G. Costello, *Nuclear Data for Reactors* Vol. 2 (1970, p. 265, IAEA Vienna).
7. V. B. Cheknokov, V. A. Tolstikov, Ju. Ja. Stavisskii, A. A. Bergman, and A. E. Samsanov, *Yadern. Fiz Iss.*, **13** 6 (1972).
8. N. Yamamuro, K. Saito, T. Emoto, T. Wada, Y. Fujita, and K. Kobayashi, *J. Nucl. Sci. and Tech.*, **17** 582 (1980).
9. G. de Saussure and A. B. Smith, *Nuclear Data for Science and Technology*, EUR 8355 (1983), p. 9.
10. H. Tellier, *Proceedings of the IAEA Consultants Meeting on Uranium Plutonium Isotopes Resonance Parameters*, INDC (NDS) - 129/GJ, p. 7 (1981).
11. Several specialist meetings were organized for the purpose of reviewing discrepancies in the ^{238}U and ^{239}Pu neutron data and their impact on nuclear energy programs. In particular "Specialist Meeting on Resonance Parameters on Fertile Nuclei and ^{239}Pu," Saclay 1974; Seminar on ^{238}U Resonance Capture, BNL 1975; "Consultants Meeting on Uranium and Plutonium Isotope Resonance Parameters," Vienna 1981; Second Jackson Hole Colloquium, "The Doppler Effect in LMFBR," Wyoming 1983. See also M. Lineberry, Kiamesha Lake ANS Topical Meeting 1981.
12. J. W. Dabbs, "Neutron Cross Section Measurements at ORELA," *Proceedings of the International Conference on Nuclear Cross Sections for Technology,* NBS Special Publication, 594 (1980).

13. D. K. Olsen, G. de Saussure, R. B. Perez, F. C. Difilippo, R. W. Ingle, and H. Weaver, *Nucl. Sci. Eng.*, **69** 202 (1979).

14. F. C. Maienschein, ORNL/TM-3833 (1972).

15. R. L. Macklin, *Nucl. Instr. and Methods*, **91**, 79 (1971).

16. E. G. Silver, J. H. Todd and J. Lewin, *Neutron Physics Division Annual Progress Report for Period Ending May 31, 1969*, ORNL-4433, p. 11 (1969); E. G. Silver, J. Lewin and J. Todd, *Neutron Physics Division Annual Progress Report for Period Ending May 31, 1968*, ORNL-4280, p. 135 (1968).

17. Nuclear Enterprises Ltd., *NE-224 Liquid Scintillator.*

18. R. L. Macklin, N. W. Hill, B. J. Allen, *Nucl. Inst. and Methods*, **96**, 509 (1971). See also B. J. Allen, R. L. Macklin, R. R. Winters, and C. Y. Fu, *Phys. Rev. C*, **8**(4), 1504 (1973).

19. J. W. Reynolds, *Data Acquisition System Hardware*, ORNL/TM-5638, Vol. 1, Oak Ridge National Laboratory.

20. N. A. Betz, J. G. Craven, D. R. Winkler, unpublished ORNL internal report (available from J. G. Craven).

21. For a more extended discussion of resolution broadening, see G. de Saussure et al. *Simultaneous Measurements of the Neutron Fission and Capture Cross Sections for* ^{235}U *for Incident Neutron Energies from 0.4 eV to 3 keV*, ORNL/TM-1804, p. 26 (1967).

22. W. E. Lamb, Jr. *Phys. Rev.*, **55**, 190 (1939).

23. A. Michaudon, *Contribution à l'ètude par des mèthodes du temps de vol de l'interaction des neutrons lents avec l'U-235*, CEA-R-2552 (1964), p. 182.

24. J. Rainwater et al., *Rev. Sci. Instr.*, **31**, 481 (1960); A. Michaudon, *Reactor Sci. Technology*, **17**, 168 (1963).

25. C. Coceva, R. Simonini, D. K. Olsen, *Nucl. Instr. and Methods*, **211**, 459 (1983).

26. We are indebted to Dr. J. A. Harvey, ORELA Facility, Oak Ridge National Laboratory for suggesting this technique and for numerous and enlightening discussions on its application.

27. R. W. Peelle, ORNL, private communication (1987).

28. M. Moxon, Harwell (U.K.), private communication (1985).

29. M. D. Drake, BNL Report No. 50274 (T-601), Vol. 1, 1970; see also Report No. BNL-NCS-50496, revised by D. Garber, C. Dunford, and S. Pearlstein, 1975 and 1976.

30. D. K. Olsen, P. S. Meszaroj, *Nucl. Sci. Eng.*, **83**, 174 (1983).

31. R. L. Macklin, ORNL, private communication (1985).

32. J. A. Harvey, ORNL, private communication (1987).

33. W. P. Poenitz, P. T. Guenther, A. B. Smith, *Proceedings of the NEANDC/NEACRP Specialist's Meeting on Fast-Neutron Capture Cross Sections*, ANL-83-4 and NEANDC (US)-214/L, April 1982.

INTERNAL DISTRIBUTION

1. R. G. Alsmiller, Jr.
2–5. G. de Saussure
6. H. Derrien
7. J. K. Dickens
8. C. Y. Fu
9. R. Gwin
10. J. A. Harvey
11–12. R. W. Ingle
13. R. L. Macklin
14–17. Roger L. Macklin
18. F. C. Maienschein
19. D. K. Olsen
20. R. W. Peelle
21. F. G. Perey
22–25. R. B. Perez
26. R. R. Spencer
27. R. R. Winters
28. L. W. Weston
29. A. Zucker
30. J. J. Dorning (consultant)
31. G. H. Golub (consultant)
32. R. M. Haralick (consultant)
33. D. Steiner (consultant)
34–35. Laboratory Records Department
36. Laboratory Records, ORNL–RC
37. Document Reference Section
38. Central Research Library
39. ORNL Patent Section

EXTERNAL DISTRIBUTION

40. Office of Assistant Manager for Energy Research and Development, U.S. Department of Energy, Oak Ridge Operations, Oak Ridge, TN 37831
41. E. D. Arthur, T-2, MS-243, Los Alamos National Laboratory, P. O. Box 1663, Los Alamos, NM 87545
42. P. Rose, Building 197D, National Nuclear Data Center, Brookhaven National Laboratory, Upton, NY 11973
43. Robert MacFarlane, T-2, MS-243, Los Alamos National Laboratory, P. O. Box 1663, Los Alamos, NM 87545
44. F. M. Mann, W/A-4, Westinghouse Hanford, P. O. Box 1970, Richland, WA 99352
45. G. L. Morgan, Los Alamos National Laboratory, P. O. Box 1663, Group P-15, MS D406, Los Alamos, NM 87545
46. R. E. Schenter, Westinghouse Hanford, P. O. Box 1970, Richland, WA 99352
47. S. L. Whetstone, Division of Nuclear Sciences, Office of Basic Energy Sciences, U.S. Department of Energy, Washington, DC 10545
48. W. P. Poenitz, Argonne National Laboratory - West, EBR-II Site, INEL, P. O. Box 1528, Idaho Falls, ID 83401
49. M. G. Sowerby, Nuclear Physics Division, B.418.15, AERE Harwell, Oxfordshire, OX11 ORA, United Kingdom
50. M. C. Moxon, Nuclear Physics Division, B.418.15, AERE Harwell, Oxfordshire, OX11 ORA, United Kingdom
51. M. S. Moore, T-2, Los Alamos National Laboratory, P. O. Box 1663, Los Alamos, NM 87545
52. George Auchampaugh, T-2, Los Alamos National Laboratory, P. O. Box 1663, Los Alamos, NM 87545
53. P. G. Young, T-2, MS-243, Los Alamos National Laboratory, P. O. Box 1663, Los Alamos, NM 87545
54–57. April Donegain, National Nuclear Data Center, ENDF, Brookhaven National Laboratory, Upton, NY 11973
58–87. Technical Information Center